



## RESEARCH ARTICLE

10.1002/2016JC012513

## Key Points:

- Initialization with observed iceberg positions and a realistic size distribution
- Drift and melt of small ( $\leq 2.2$  km length) to giant icebergs ( $\geq 10$  km) is simulated
- Including larger icebergs leads to a northward shift of the freshwater input with reduced seasonality

## Correspondence to:

T. Rackow,  
thomas.rackow@awi.de

## Citation:

Rackow, T., C. Wesche, R. Timmermann, H. H. Hellmer, S. Juricke, and T. Jung (2017), A simulation of small to giant Antarctic iceberg evolution: Differential impact on climatology estimates, *J. Geophys. Res. Oceans*, 122, doi:10.1002/2016JC012513.

Received 27 OCT 2016

Accepted 19 MAR 2017

Accepted article online 23 MAR 2017

## A simulation of small to giant Antarctic iceberg evolution: Differential impact on climatology estimates

Thomas Rackow<sup>1</sup> , Christine Wesche<sup>1</sup>, Ralph Timmermann<sup>1</sup>, Hartmut H. Hellmer<sup>1</sup>, Stephan Juricke<sup>2</sup>, and Thomas Jung<sup>1,3</sup>

<sup>1</sup>Alfred Wegener Institute, Helmholtz Centre for Polar and Marine Research, Bremerhaven, Germany, <sup>2</sup>Atmospheric, Oceanic and Planetary Physics, University of Oxford, Oxford, UK, <sup>3</sup>Institute of Environmental Physics, University of Bremen, Bremen, Germany

**Abstract** We present a simulation of Antarctic iceberg drift and melting that includes small, medium-sized, and giant tabular icebergs with a realistic size distribution. For the first time, an iceberg model is initialized with a set of nearly 7000 observed iceberg positions and sizes around Antarctica. The study highlights the necessity to account for larger and giant icebergs in order to obtain accurate melt climatologies. We simulate drift and lateral melt using iceberg-draft averaged ocean currents, temperature, and salinity. A new basal melting scheme, originally applied in ice shelf melting studies, uses in situ temperature, salinity, and relative velocities at an iceberg's bottom. Climatology estimates of Antarctic iceberg melting based on simulations of small ( $\leq 2.2$  km), "small-to-medium-sized" ( $\leq 10$  km), and small-to-giant icebergs (including icebergs  $> 10$  km) exhibit differential characteristics: successive inclusion of larger icebergs leads to a reduced seasonality of the iceberg meltwater flux and a shift of the mass input to the area north of 58°S, while less meltwater is released into the coastal areas. This suggests that estimates of meltwater input solely based on the simulation of small icebergs introduce a systematic meridional bias; they underestimate the northward mass transport and are, thus, closer to the rather crude treatment of iceberg melting as coastal runoff in models without an interactive iceberg model. Future ocean simulations will benefit from the improved meridional distribution of iceberg melt, especially in climate change scenarios where the impact of iceberg melt is likely to increase due to increased calving from the Antarctic ice sheet.

**Plain Language Summary** Antarctic icebergs are large blocks of frozen fresh water that melt around the Antarctic continent while moving under the influence of winds, sea ice, and ocean currents. Small icebergs ( $\leq 2.2$  km) are mainly driven by winds and ocean currents, whereas giant icebergs ( $> 10$  km) tend to 'surf' the tilted sea surface and are less sensitive to changes in the wind. The relative importance between melting at the iceberg's base and mass loss at the side walls is also different for small and large icebergs. We present a computer simulation of Antarctic iceberg movement and melting that includes not only small icebergs, but at the same time also larger icebergs with side lengths of 10 km or more. The study highlights the necessity to account for larger icebergs in order to obtain an accurate depiction of the spatial distribution of iceberg meltwater, which, e.g., stabilizes and fertilizes the upper water column and thus supports phytoplankton growth. Future climate change simulations will benefit from the improved distribution, where the impact of iceberg melting is likely to increase due to increased calving from the Antarctic ice sheet.

© 2017. The Authors.

This is an open access article under the terms of the Creative Commons Attribution-NonCommercial-NoDerivs License, which permits use and distribution in any medium, provided the original work is properly cited, the use is non-commercial and no modifications or adaptations are made.

### 1. Introduction

Iceberg calving is an important component of the mass balance of the Antarctic Ice Sheet. In the early 1990s, iceberg calving has been overestimated due to the lack of in situ observations [Jacobs *et al.*, 1992]. With the advances in remote sensing capabilities, recent estimates of  $\sim 1300$  Gt/yr (1 Gt =  $10^{12}$  kg) are similar to the mass loss caused by ice shelf basal melting [Depoorter *et al.*, 2013]. As the iceberg mass ultimately melts within the waters surrounding Antarctica, it represents an important component of the Southern Ocean freshwater cycle. The total mass is usually assumed to be evenly divided between giant icebergs

(length  $\geq 10$  km) and smaller ones, with some estimates preferring giant icebergs (as high as 89%) [Stern *et al.*, 2016].

Once afloat, icebergs interact with the ocean and sea ice. They serve as obstacles for the sea ice drift [Hunke and Comeau, 2011], causing accumulation and thickening on the windward side but open water (polynyas) on the lee side. The latter has a strong influence on biological productivity and, thus, on the sequestration of atmospheric CO<sub>2</sub> [e.g., Arrigo *et al.*, 2008] as well as on the densification of the shelf water masses and the ventilation of the deep ocean [Tamura *et al.*, 2016]. Furthermore, iceberg wall melting drives local upwelling from beneath the pycnocline. This contributes to the fertilization of the euphotic zone due to “dust nutrients” in the glacial melt, and to the stabilization of the water column, both supporting phytoplankton growth [Stern *et al.*, 2015; Duprat *et al.*, 2016]. Although a comparatively small effect, the cooling and freshening might also impact on ocean density and, thus, sea level rise [Jenkins and Holland, 2007].

In turn, icebergs may ground in shallow areas or get locked into a compact sea ice cover. In the latter case, sea ice may transport icebergs faster due to the larger “sail” a solid sea ice cover provides for the wind [Lichey and Hellmer, 2001; Schodlok *et al.*, 2006]. Being immersed in the ocean, icebergs are facing three main mechanisms of decay: basal melting; buoyant convection along the sides, leading to a transfer of heat; and lateral erosion due to ocean waves, which is often the dominant process [Gladstone *et al.*, 2001].

Icebergs also pose a hazard to human installations, such as oil platforms and submarine pipelines. The threat of drifting icebergs for shipping remains high since the historical sinking of RMS Titanic in 1912, as demonstrated by the collision of the Antarctic cruise liner “Explorer” with an iceberg in 2007, and might even increase in the future [Bigg and Wilton, 2014]. Last but not least, considering the shortage in drinking water in the southern hemisphere, freshwater from icebergs might be used in the future for the irrigation of formerly fertile farmland.

Previous iceberg model studies either (a) focused on small icebergs up to a side length of 2.2 km [e.g., Gladstone *et al.*, 2001; Merino *et al.*, 2016], (b) combined numerical simulations of small icebergs with available observations of giant icebergs [Silva *et al.*, 2006], or (c) studied solely the drift of single giant icebergs without considering their melt [Lichey and Hellmer, 2001; Hunke and Comeau, 2011]. Model-based iceberg melt climatologies, considering small icebergs up to lengths of 2.2 km, typically rely on prescribed climatological calving rates as boundary conditions with the advantage of using a realistic total mass flux (in Gt/yr). However, it remains an open question how best to partition the overall mass flux in models between (i) the different calving sites around Antarctica and (ii) the different iceberg size classes (in number of icebergs per year). A realistic treatment would require separate size distributions for every Antarctic calving site [Wesche *et al.*, 2013], including calving of icebergs larger than 2.2 km (or even 10 km) at certain sites. This makes it even more complex since the calving of giant icebergs is less frequent, is currently not possible to forecast, and happens on decadal timescales. Consequently, the calving of giant icebergs might need to be treated in models as a random process similar to volcanic eruptions in historical climate simulations [Stern *et al.*, 2016].

Introducing 10 iceberg size classes up to side lengths of 2.2 km (still considered “small” in the present study), Stern *et al.* [2016] show an increase of the westward transport of iceberg melt with the Antarctic coastal current if more weight is given to the calving of “larger” icebergs. Meridionally, according to Silva *et al.* [2006], 35% (3%) of the mass of giant (small) icebergs in the Southern Ocean is transported north of 63°S, indicating that small icebergs preferably melt close to the Antarctic coast. Ideally, climatology estimates of iceberg melt should also consider the drift and melt of giant icebergs in order to circumvent systematic biases.

Here we complement a global ocean-sea ice model focused on the Southern Ocean, which includes the explicit simulation of all major Antarctic ice shelf cavities, by an iceberg drift and decay model. For the first time, an iceberg model is initialized with an observed near-coastal iceberg size distribution, which comprises a wide spectrum, ranging from small to giant icebergs. The chosen iceberg model setup thus resembles an initial value problem (instead of a boundary value problem) in some respect, so that our methodology for the estimation of a climatological meltwater flux can be considered a novel approach. Drift and decay of the icebergs is simulated for 12 years and several melt climatology estimates are produced.

The paper is organized as follows: section 2 describes the setup of the iceberg model and the underlying sea ice-ocean model, as well as the initialization with the near-coastal data set of icebergs, categorized into

five iceberg classes. Section 3 analyzes the simulated iceberg melting for the different size classes and compares the overall simulated drift to observed iceberg trajectories. The different dynamics for small and giant icebergs in ice-free conditions in the Antarctic coastal current is also discussed. Meltwater climatology estimates based on only small, small-to-medium-sized, and small-to-giant icebergs are given in section 4 and compared to another recent estimate. A summary and conclusion is given in section 5.

## 2. Model Setup

### 2.1. Overview

We use the Finite Element Sea ice-Ocean Model (FESOM) [Timmermann *et al.*, 2009; Wang *et al.*, 2014] developed at the Alfred Wegener Institute (AWI) in the “ice shelf” configuration introduced by Timmermann *et al.* [2012]. Ice shelf melting around Antarctica is explicitly simulated in this model, and its basic configuration is briefly described below. For this study, a dynamic-thermodynamic iceberg model [Rackow, 2011] has been directly embedded into the FESOM code, partly because of the strong dependence of iceberg drift on the three-dimensional ocean current fields (for surface currents versus depth-integrated ocean velocities, see Merino *et al.* [2016, Figure 2]), but also to allow for a more straightforward coupling of three-dimensional melt fields into the temperature and salinity budget in future versions of the model. At present, a one-way coupling is used, so that the modeled ocean does not respond to the melting and cooling from icebergs. The iceberg model is forced “online” with current ice-ocean fields at every time step from the FESOM model during run time. Several successful attempts of fully coupled iceberg modeling have been made already [Jongma *et al.*, 2009; Martin and Adcroft, 2010], but these have considered direct interaction only with the surface ocean layer. Possible feedbacks arising from a coupling of three-dimensional melt fields could be addressed in future studies with FESOM-IB.

Our goal is to reproduce the overall drift pattern of icebergs of various size classes around Antarctica, leading to the use of a single set of established model parameters and drag coefficients. In order to optimize for single observed trajectories, however, tuning would be required for every single iceberg [e.g., Keghouche *et al.*, 2009; Rackow, 2011].

### 2.2. FESOM Configuration

We use the FESOM configuration introduced by Timmermann *et al.* [2012] as the parent model to force the iceberg component. This model includes the three-equation approach of ice shelf basal melting [Hellmer and Olbers, 1989; Holland and Jenkins, 1999] and provides a good representation of ocean circulation, sea ice properties, and ice shelf basal melt rates [Timmermann *et al.*, 2012]. Horizontal resolution in this configuration varies between 7 km under the large ice shelves in the Ross and Weddell Seas and about 250 km in the vast basins of the Atlantic and Pacific Oceans. The resolution in the offshore Southern Ocean varies between 30 and 40 km [Timmermann *et al.*, 2012]. A time step of 3 min is applied. The FESOM simulation is forced with the interannually varying CORE.v2 forcing [Large and Yeager, 2009], which has a horizontal resolution of  $\sim 2^\circ$  and is available for the period 1948–2008. After a 10 year spinup, icebergs are initialized in the model year 1997 (see section 2.4).

### 2.3. The Iceberg Module

The IceBerg module (IB) [Rackow, 2011] for FESOM is based on established iceberg physics from Smith and Banke [1983], Bigg *et al.* [1997], Gladstone *et al.* [2001], and additions by Lichey and Hellmer [2001] to improve the drift simulation of giant icebergs.

Continuing on these studies, depth-integrated velocities from the vertical current profile were already used in the first model version by Rackow [2011]. Some further nonstandard additions have been implemented for the present study: a new basal melting scheme and the use of vertical profiles of temperature (and salinity), which is essential for modeling the melting of icebergs with large drafts. We briefly repeat the basic physics that govern the drift and decay of icebergs and describe the novel additions for this study. Those readers solely interested in the results of the iceberg drift and melt analysis are referred to sections 3 and 4.

#### 2.3.1. Dynamics

Icebergs in the model are treated as Lagrangian particles carrying physical properties such as mass  $M$ , height  $H$ , and length  $L$  that are adapted in the course of the simulation due to melting and erosion (see section 2.3.3). To simplify the observed complex iceberg shapes, we assume icebergs to be cuboids with

surface area  $A_{skin} = L^2$ . The total height ( $H$ ) is split into the submerged part  $D$  (draft or keel depth) and the freeboard  $F$  above water ( $H = F + D$ ). The draft follows from  $H$  using Archimedes' principle  $D = H\rho/\rho_o$ , where  $\rho = 850 \text{ kg/m}^3$  is a density typical for icebergs in the Southern Ocean [Silva et al., 2006] and  $\rho_o = 1027.5 \text{ kg/m}^3$  is an average density for seawater.

The iceberg momentum balance is solved for the iceberg velocity  $\mathbf{u}$  and follows from a superposition of all forces acting on an iceberg,

$$M \frac{d\mathbf{u}}{dt} = \mathbf{F}_c + \mathbf{F}_{sl} + \mathbf{F}_a + \mathbf{F}_o + \mathbf{F}_i, \quad (1)$$

where  $d/dt$  is the material time derivative including advection of momentum,  $\mathbf{F}_c = -Mf \times \mathbf{u}$  is the Coriolis force with parameter  $f$ , and  $\mathbf{F}_{sl} = -Mg\nabla\eta$  is the downward force along a sea surface height ( $\eta$ ) slope due to the gravitational acceleration  $g$  of Earth. These two body forces are complemented by surface forces  $\mathbf{F}_x$ , namely oceanic (subscript  $x = o$ ) and atmospheric ( $x = a$ ) drags of the general form

$$\mathbf{F}_x = C_x |\mathbf{u}_x - \mathbf{u}| (\mathbf{u}_x - \mathbf{u}), \quad (2)$$

where  $|\cdot|$  is the vector norm,  $\mathbf{u}_x$  the ambient velocity (currents or winds) at the location of the iceberg, and  $C_x = \rho_x (0.5 C_x A_x + c_{skin,x} A_{skin})$  is a drag coefficient summing the contribution from skin drag (acting on the surface/bottom  $A_{skin}$ ) and form drag (acting on the area  $A_x$  perpendicular to the flow) [Smith and Banke, 1983]. The drag coefficients are thus changing in time due to melting of the iceberg. The drags are only applied to drive an iceberg, with no feedback on the surroundings.

1. In case of the ocean drag  $\mathbf{F}_o$ ,  $A_o = DL$  is the submerged area of a sidewall and  $c_o = 0.85$  [Lichey and Hellmer, 2001]. The skin drag coefficient is set to the value for the ocean-sea ice drag coefficient in the FESOM code,  $c_{skin,o} = 5 \times 10^{-3}$ , which is 1 order of magnitude larger than in Lichey and Hellmer [2001] but close to the choice of Keghouche et al. [2009]. The ocean velocity  $\mathbf{u}_o$  is set to the vertical mean of the ocean velocity profile over the iceberg draft  $D$ . A similar dependence on the depth-averaged ocean currents has recently been implemented in other studies [Marsh et al., 2015; Merino et al., 2016] and was found to significantly affect trajectories of thicker icebergs, especially in the Weddell Sea.
2. For the atmospheric drag  $\mathbf{F}_a$ ,  $A_a = FL$  is the area of a sidewall above sea level,  $\rho_a = 1.293 \text{ kg/m}^3$ ,  $c_a = 0.4$  following Lichey and Hellmer [2001] and  $c_{skin,a} = 2.5 \times 10^{-3}$  (again similar to Keghouche et al. [2009]). We do not consider a wave radiation force [Smith, 1993] in our simulation (although implemented in the model), mainly because there is still scientific debate about its formulation. Broström et al. [2009] introduced a wave radiation coefficient of  $C_{wave} = 0.3$  to the original formulation by Smith [1993]. Martin and Adcroft [2010, discussion in Appendix A] had to introduce an even smaller (and variable) coefficient in order to stabilize their model. Since the force is in the same direction as the atmospheric drag, the effect of ocean surface waves created by the wind could be implicitly accounted for by choosing a higher atmospheric drag coefficient [Smith, 1993; Keghouche et al., 2009].
3. The sea ice force  $\mathbf{F}_i$  is split into different cases, depending on the ice concentration  $A$  and sea ice strength  $P$  as introduced by Lichey and Hellmer [2001],

$$\mathbf{F}_i = \begin{cases} 0, & \text{if } A \leq 15\% \\ 0.5c_i\rho_i A_i |\mathbf{u}_i - \mathbf{u}| (\mathbf{u}_i - \mathbf{u}), & \text{if } A > 15\% \text{ and } (A < A_s \text{ or } P < P_s) \end{cases}. \quad (3)$$

Under most circumstances, an iceberg will be either subject to a generally small sea ice drag, where  $c_{skin,i} = 0$  and  $c_i = 1.0$  [Bigg et al., 1997],  $\rho_i = 910 \text{ kg/m}^3$  [Timmermann et al., 2009], and  $A_i = Lh_i$  with  $h_i$  the ice thickness at the location of the iceberg; or the iceberg will be in open water ( $A \leq 15\%$ ) and will thus not be subject to any sea ice force. However, sea ice may "capture" icebergs in severe conditions when both the sea ice concentration  $A$  and the sea ice strength  $P$  reach higher values than some thresholds  $A_s$  and  $P_s$ . In this third case, i.e., if  $A \geq A_s$  and  $P \geq P_s$ , sea ice is considered strong enough to counteract all other forces; the iceberg velocity  $\mathbf{u}$  is then simply set to the sea ice velocity  $\mathbf{u}_i$ , effectively bypassing the momentum equation. We choose a threshold of  $A_s = 90\%$ , as in the original formulation by Lichey and Hellmer [2001], but a somewhat smaller value of  $P_s = 10,000 \text{ N m}^{-1}$  to account for the average sea ice strength being generally lower in our simulations.

Note that the “capturing” by sea ice is formulated in a discontinuous if-else manner, which can lead to numerical difficulties. As a regularization to equation (3) and the third case explained above, *Martin and Adcroft* [2010] propose to use a sea ice drag formulation with a coefficient that increases exponentially with sea ice concentration. However, as this approach neglects the dependence on sea ice strength, we chose an alternative formulation using a regime function based on two linear functions [*Rackow*, 2011, pp. 63–65]. As a result, sea ice starts influencing the iceberg velocity at  $A = 86\%$  and  $P = 8000 \text{ N m}^{-1}$ , exerting increasing control until the thresholds  $A_s$  and  $P_s$  are reached. The value  $A = 86\%$  is motivated by observations from *Schodlok et al.* [2006] who show that the capturing of icebergs by sea ice can occur at those concentrations.

Due to strong erosion at the sides (see section 2.3.3), the simulated icebergs are reduced to a column-like shape with time. At some point, icebergs will roll over according to a stability criterion [*Bigg et al.*, 1997], i.e., if

$$L < \sqrt{0.92H^2 + 58.32H}, \quad (4)$$

following the original formulation by *Weeks and Mellor* [1978, equation 9]. The iceberg height  $H$  is then set to the current value of the iceberg length  $L$ ; afterward, the iceberg length  $L$  is adjusted so that the iceberg volume is conserved retaining a quadratic surface area.

Whenever the iceberg draft reaches deeper than the local bathymetry, icebergs are grounded and their velocity is set to zero. During this time, icebergs may melt until they start floating again. Moreover, whenever the center of an iceberg tries to leave the model domain, a tangential velocity to the local coastline is computed, allowing the iceberg to “creep” along the coast [*Martin and Adcroft*, 2010].

### 2.3.2. Notes on the Point Assumption

Icebergs are treated as Lagrangian (infinitesimal) points, which is an assumption generally made in iceberg models; the consequences of the assumption are detailed below. We also describe our approach how to treat the possible breakdown of this assumption for giant icebergs.

The areal coverage of icebergs in the model is zero, implying that groups of icebergs can theoretically occupy more (virtual) area than the grid cell they are situated in. Furthermore, iceberg-iceberg interactions, e.g., collisions, are not accounted for. The point assumption necessitates further assumptions on the iceberg orientation in the flow (i.e., on the surfaces the various forces are acting on, see section 2.3.1).

Giant iceberg dynamics is largely controlled by the sea surface tilt force, and only to a lesser degree by the drag forces (section 3.3). We compute a weighted mean of  $\nabla\eta$  over the surrounding elements before computing  $\mathbf{F}_{sl}$ , motivated by the fact that icebergs greater than the grid spacing should be able to “feel” the slope of surrounding elements. Besides being physically plausible, this also avoids a zig-zag behavior of modeled iceberg trajectories arising from the fact that the sea surface slope is discontinuous over element edges according to the finite element discretization of  $\eta$  in FESOM. As intended, this change mainly impacts giant icebergs, because the sea surface slope is of minor importance in the dynamics of small icebergs (see also section 3.3).

### 2.3.3. Thermodynamics and Erosion

The thermodynamics of icebergs in current models is based on simple diagnostic and mostly empirical equations [*Bigg et al.*, 1997; *Gladstone et al.*, 2001; *Martin and Adcroft*, 2010]. It comprises three main processes, (1) the basal melting of icebergs at the bottom  $M_b$  (and at the submerged sides,  $M_{bv}$ ); (2) Bouyant convection  $M_v$  along the sides of an iceberg due to the temperature difference between ice and ocean, leading to a transfer of heat; and (3) erosion on the sides due to waves and associated calving of overhanging slabs,  $M_e$ . The mass balance for an iceberg is thus given by

$$\rho \frac{dV}{dt} = -\rho(A_b M_b + A_{bv} M_{bv} + A_v M_v + A_e M_e), \quad (5)$$

where  $V$  is the iceberg volume and the rates of melting and erosion (in  $\text{m s}^{-1}$ ) have been multiplied by the respective areas they are acting on:

1. Erosion by surface waves is assumed to act on two sidewalls, i.e.,  $A_e = 2LH$ . This process is described by the empirical formulation

$$M_e = \frac{1}{12} c_{M_e} (T_o + 2^\circ\text{C}) [1 + \cos(A^3 \pi)] S_s, \quad (6)$$

where  $T_o$  is the sea surface temperature in  $^\circ\text{C}$ .  $S_s$  is the (dimensionless) sea state as a function of the relative velocity between winds and the ocean,  $S_s = \frac{3}{2} |(\mathbf{u}_a - \mathbf{u}_o) \frac{s}{m}|^2 + \frac{1}{10} |(\mathbf{u}_a - \mathbf{u}_o) \frac{s}{m}|$ , following from a fit to

the Beaufort scale [Martin and Adcroft, 2010]. We introduced the coefficient  $c_{M_e} = m (86400 \text{ s } ^\circ\text{C})^{-1}$  to ensure units of  $\text{m s}^{-1}$ . The impact of surface waves is damped with increasing sea ice cover according to the factor  $[1 + \cos(A^3\pi)]$ . Damping starts at sea ice concentrations around 40%, with increasing influence toward concentrations of 100%, where  $[1 + \cos(A^3\pi)]$  is zero. The factor follows personal observations by Gladstone et al. [2001] in the Weddell Sea in 1999. The wave erosion term is in many cases the most important term leading to the decay of icebergs in the simulations, but probably the least constrained process considered. Ideally, future research should therefore focus on better constraining this term, building on the initial work by Bigg et al. [1997] and Gladstone et al. [2001].

2. Bouyant convection results in a comparatively smaller melt rate  $M_v$  along the iceberg's sidewalls, i.e.,  $A_v = 4LD$ . It is described by

$$M_v = c_{M_v} (7.62 \cdot 10^{-3} \text{ } ^\circ\text{C} + 1.29 \cdot 10^{-3} T_d) T_d, \quad (7)$$

where  $T_d$  is the "thermal driving" temperature, defined as the "elevation of ambient water temperature above freezing point"  $T_f$  [Neshyba and Josberger, 1980]. As before,  $c_{M_v} = m (86400 \text{ s } ^\circ\text{C}^2)^{-1}$  ensures units of  $\text{m s}^{-1}$ .  $T_d$  is often set to the sea surface temperature [Bigg et al., 1997; Martin and Adcroft, 2010] with the implicit assumption  $T_f = 0$  and neglecting any subsurface temperature distribution. We do not follow this approach; instead, we follow the original formulation by Neshyba and Josberger [1980] more closely and set  $T_d = \max(0, T_m - T_f)$ , where  $T_f$  is the in situ freezing temperature at middepth  $D/2$ , and  $T_m$  is the average water temperature in  $^\circ\text{C}$  along the iceberg draft  $D$ .  $T_m$  can be considered to represent the water temperature at middepth  $D/2$ .

3. Basal melting is especially important for giant icebergs. In the computation of the respective melt rate  $M_b$  (and the lateral "basal" melt rate  $M_{bv}$ ), our model differs from the studies by Bigg et al. [1997], Gladstone et al. [2001], and Martin and Adcroft [2010]. Instead, we chose the physically better constrained three-equation formulation, originally introduced by Hellmer and Ollbers [1989] and Holland and Jenkins [1999] for melting at an ice shelf base. A system of three equations is solved for temperature and salinity in the boundary layer at the interface between an iceberg and the ocean, and for the associated melt rates at the iceberg's bottom and at its submerged sides given far-field temperatures and salinities. While generally a melt rate, the formulation can lead to negative values in some situations, resulting in slightly increasing iceberg mass (which is akin to refreezing occurring at the base of some ice shelves).

We apply the available ice shelf basal melting implementation in FESOM [Timmermann et al., 2012] and adapt it to the iceberg case: a "basal" melt rate is computed separately at both the bottom ( $A_b = L^2$ ) and at the submerged sides of an iceberg ( $A_{bv} = A_v = 4LD$ ), motivated by Bigg et al. [1997, p. 117] who note that "basal" turbulent heat transfer also occurs on the sides of the berg past which the water flows." For the lateral turbulent melting, far-field temperature and salinity values in middepth  $D/2$  ( $T_m$  and  $S_m$ ) are determined by averaging over the iceberg draft. Far-field temperature and salinity values at the bottom of the iceberg ( $T_{\text{keel}}$  and  $S_{\text{keel}}$ ) are determined via linear interpolation between adjacent model levels to depth  $D$  and are then used for the turbulent melting at the iceberg bottom. Since the coefficients of the turbulent heat fluxes depend on the friction velocity as in Jenkins [1991], we set the friction velocity to the relative velocity between the iceberg and the ocean ( $|\mathbf{u}_o - \mathbf{u}|$ ) for lateral melting, where  $\mathbf{u}_o$  is the draft-averaged ocean current, and  $|\mathbf{u}_{\text{keel}} - \mathbf{u}|$  for bottom melting, where  $\mathbf{u}_{\text{keel}}$  is the ocean velocity at the iceberg bottom).

## 2.4. Initialization

Recently, a data set of circum-Antarctic iceberg positions and dimensions became available that can be utilized to initialize an iceberg model along the coast: Wesche and Dierking [2015] determined a large number of near-coastal iceberg positions and associated horizontal dimensions for September/October 1997. While climatological calving rates ensure a realistic long-term mass flux but not necessarily a realistic size distribution at any single instant in time, the Wesche and Dierking [2015] data set is a single most realistic realization of the actual size distribution of near-coastal icebergs.

### 2.4.1. Coverage

The data set is based on a satellite product originally intended for mapping the Antarctic continent, not primarily the coastal ocean. Still, the data set covers 100% of the global near-coastal area up to 20 km offshore; for distances up to 100 km the global coverage continues to be about 96%. While this suggests an extensive global coverage of the near-coastal regions, Wesche and Dierking [2015] note that the coverage along the Antarctic Peninsula in the Weddell Sea, the "iceberg alley," does not exceed 20 km in some places, so that

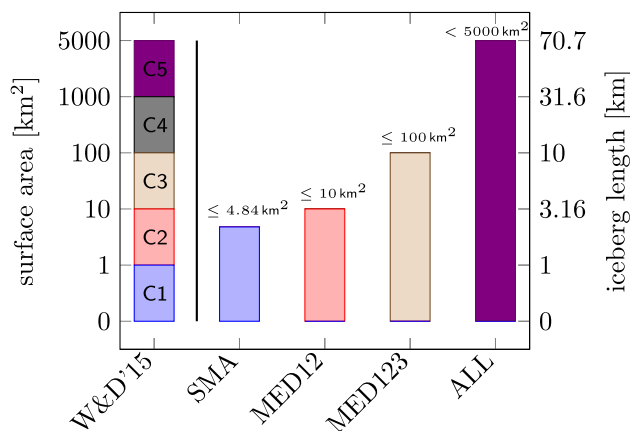


**Figure 1.** Definition of the iceberg size classes used in this study. Left column: five size classes C1–C5 defined in *Wesche and Dierking* [2015] (W&D'15). Right column: four additional classes introduced here for the estimation of melt climatologies. “SMA” comprises small icebergs up to side lengths of 2.2 km, which corresponds to 4.84 km<sup>2</sup>; “MED12” (“MED123”) is based on the medium-sized icebergs in classes C1 and C2 (C1–C3); “ALL” comprises all five classes, including giant icebergs from classes C4 and C5.

smaller icebergs will be generated in the course of the simulation due to melting whereas larger icebergs would remain absent. Following *Wesche and Dierking* [2015], the iceberg height is set to 250 m (a more conservative value than the 360 m also discussed in their study), summing up to a total initial iceberg mass of 5167 Gt.

*Wesche and Dierking* [2015] classified the icebergs into five size classes, according to their surface area (Figure 1): 0–1 km<sup>2</sup> (class C1), 1–10 km<sup>2</sup> (class C2), 10–100 km<sup>2</sup> (class C3), 100–1000 km<sup>2</sup> (class C4), and 1000–5000 km<sup>2</sup> (class C5); the smallest iceberg in C1 has a surface area of 0.3 km<sup>2</sup> (i.e.,  $\approx(550 \text{ m})^2$  following from the SAR restrictions given above), the largest iceberg in C5 has a surface area of 4717.6 km<sup>2</sup> [*Wesche and Dierking*, 2015]. Classes C1–C3 comprise 6892 icebergs while classes C4 and C5 comprise only 20 (giant) icebergs. Consequently, 0.3% of the icebergs (the giant icebergs in classes C4 and C5) carry about 60% of the initial mass, whereas the remaining 99.7% of the icebergs carry only 40%.

As mentioned before, the calving of giant icebergs is, in some respect, analogous to volcanic eruptions in climate models [*Stern et al.*, 2016] and, therefore, giant icebergs need to be somehow prescribed in models. One possible way of doing this is to initialize the model with a data set similar to that of *Wesche and Dierking* [2015], which contains giant iceberg positions and dimensions. We realize, however, that near-coastal iceberg distributions are potentially subject to temporal variation, i.e., to seasonal and interannual variability. The degree to which the near-coastal iceberg conditions of September/October 1997 are representative for other years is arguably higher for smaller icebergs, which calve comparatively frequently, with some interannual modulation, and add up to a statistically large number. The calving of giant icebergs is, however, a rare event and occurs on decadal timescales. It is therefore impossible to define instantaneous giant iceberg positions that are representative for all years in present-day climate; consequently, initialization with the *Wesche and Dierking* [2015] data set as one particular realization of the iceberg size distribution aims at highlighting the importance to include giant icebergs into meltwater estimates by taking the example of the decade following 1997.

### 3. Simulated Drift and Iceberg Melting

#### 3.1. Overview

The drift and decay of Antarctic icebergs is initialized in September 1997 and simulated for more than 11 years until December 2008. The chosen model setup with initialization from observed near-coastal iceberg positions (instead of using, alternatively, climatological calving rates as boundary conditions), without the release of new icebergs in the model, entails a decrease of the total iceberg mass until the end of the simulation.

the near-coastal iceberg mass in the Weddell Sea is likely underestimated compared to the actual conditions in September/October 1997. Going further to the north, the offshore area up to 200 km has a 74% coverage, while only half (52%) is covered up to a distance of 300 km.

#### 2.4.2. Iceberg Sizes

Using this data set, the iceberg model is initialized on 29 September 1997 with 6912 observed iceberg positions and sizes. Due to the given SAR resolution of 100 m, the smallest iceberg size that can be reliably detected is about 550 m [*Wesche and Dierking*, 2015]. We consider the lack of even smaller icebergs in the initial distribution to be of minor concern compared to the lack of larger icebergs in previous studies [*Gladstone et al.*, 2001; *Merino et al.*, 2016], since

For comparison of the model results, observed giant iceberg trajectories from the Antarctic Iceberg Tracking Database composed at Brigham Young University (BYU) are used [Stuart and Long, 2011]. In particular, we consider iceberg tracks for the period July 1999 to November 2009 from the QuikSCAT portion of the BYU database (available for download at [www.scp.byu.edu/data/iceberg/database1.html](http://www.scp.byu.edu/data/iceberg/database1.html)). To get an impression of the observed drift of smaller icebergs, we also include tracks of icebergs tagged with GPS buoys in January 2000 and January 2002 by Schodlok *et al.* [2006].

### 3.2. Trajectories

Generally, the model reproduces the large-scale drift of Antarctic icebergs as determined from the observed iceberg tracks well, with three major windmill-like branches indicative of northward iceberg drift (Figure 2): In the Weddell Sea, in the Ross Sea around 180°E, and near the Kerguelen Plateau between 60°E and 90°E. The branch in the Weddell Sea splits into two extensions, a major branch called iceberg alley along the Antarctic Peninsula into the Antarctic Circumpolar Current (ACC), and a minor one near the Neumayer-Station at the Greenwich meridian. The latter branch is solely populated by smaller icebergs of classes C1–C3. Independent of iceberg size, the dominant iceberg velocity component becomes zonal (eastward) as soon as icebergs enter the ACC.

Several trajectories from classes C3–C5 appear to be longer in the model than expected from the observed iceberg tracks. However, we argue that the modeled trajectories are not necessarily overly long because the observed trajectories are systematically shorter than in reality because of two factors: (1) GPS buoys as deployed by Schodlok *et al.* [2006] stop transmitting when falling into the ocean (this happens when an iceberg capsizes or disintegrates into smaller parts); (2) giant iceberg tracks determined from satellites end as soon as the iceberg size approaches values below some threshold, e.g., the typical limit of ~5–6 km [Stuart and Long, 2011]. This argument is supported by the observed trajectory of an iceberg that circumnavigated Antarctica, tagged in January 1999 by Schodlok *et al.* [2006] (red line in Figure 2, right), showing that icebergs can indeed travel remarkably long distances in reality. Moreover, occasional iceberg sightings along the coast of New Zealand and off the coast of South America suggest that even the most northward reaching modeled trajectories are plausible. Further evaluation of the modeled trajectories is done implicitly in section 4.4, where the simulated meltwater patterns are compared to the pattern from another modeling study.

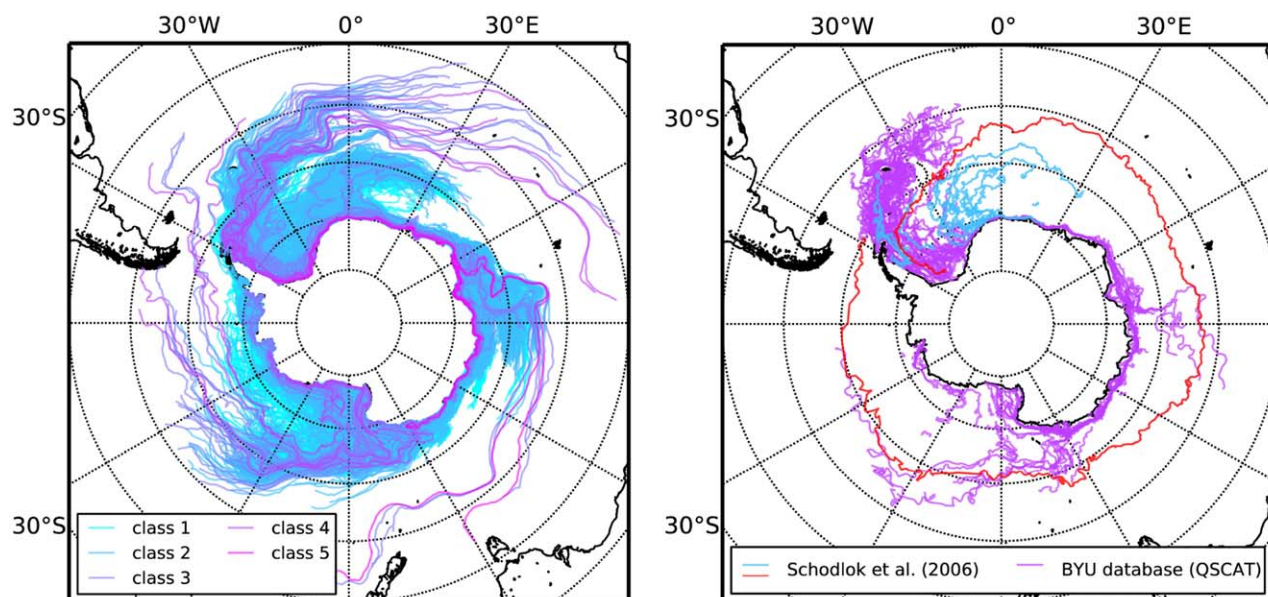


**Figure 2.** (left) All modeled iceberg trajectories for the full 12 year simulation, colored differently for better distinction of the five size classes introduced by Wesche and Dierking [2015]. (right) Observed giant iceberg trajectories (July 1999 to November 2009) from the QuikSCAT portion of the Antarctic Iceberg Tracking Database [Stuart and Long, 2011], composed at Brigham Young University (BYU), and several tracks of smaller icebergs tagged with GPS buoys in January 2000 and January 2002 by Schodlok *et al.* [2006]. A single remarkable trajectory of an iceberg that circumnavigated Antarctica (tagged in January 1999) is also shown (red line).

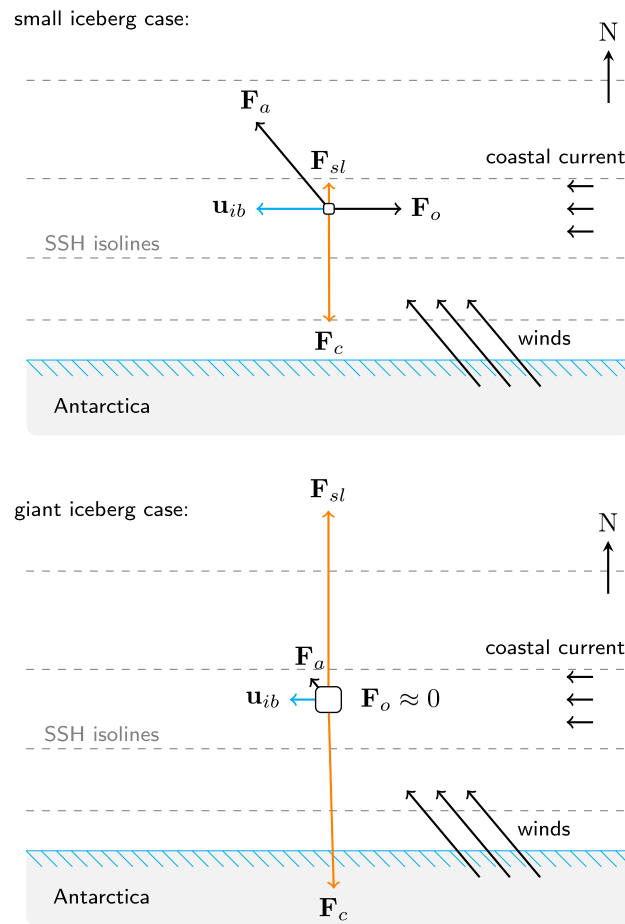


**Figure 3.** Schematic showing the typical balance between body and surface forces (orange and black arrows) for icebergs drifting in the coastal current. The balance is strongly dependent on the iceberg size: (top) for small icebergs in sea ice-free regions the balance is mainly between surface forces (atmospheric drag  $F_a$  and oceanic drag  $F_o$ ) and Coriolis  $F_c$ . Small icebergs are thus sensitive to the wind forcing, often resulting in northward drift; (bottom) for giant icebergs, the balance shifts to the body forces  $F_{sl}$  and  $F_c$ . Giant icebergs thus “surf” the tilted sea surface at velocities  $u_{ib}$  (blue) that are close to the ocean velocity, following the isolines of sea surface height (SSH), and are less sensitive to changes in the wind. The top figure for small icebergs is inspired by Gladstone *et al.* [2001, Figure 7].

to the surface slope is the only body force that drives (giant) icebergs, modeled trajectories and velocities in sea ice-free regions depend strongly on the strength of the gyres in the underlying model (compare also Lichey and Hellmer [2001]). Sensitivity studies with an earlier model version of FESOM-IB [Rackow, 2011] showed a large impact of the sea surface slope  $\nabla\eta$  already on smaller icebergs in some critical regions: a doubling of the slope in  $F_{sl}$  led to higher iceberg velocities and more icebergs crossing the Weddell Sea, leaving the coast between 20 and 30°W, as observed.

In contrast, the oceanic and atmospheric surface drags scale with the surface area they are acting on, which does not increase as quickly with iceberg size as volume (and hence mass). As a result, those forces are mainly important for smaller icebergs (Figure 3, top). Simulations by Rackow [2011] showed that, in general, the atmospheric drag is the main driving force for smaller icebergs and favors northward drift, whereas the oceanic drag acts as a friction term.

### 3.4. Decrease of Iceberg Mass

Starting from the initial conditions by Wesche and Dierking [2015] in September 1997, the total iceberg mass decreases over the course of the simulation until almost all icebergs have melted after about a decade

### 3.3. Comparing Small to Giant Iceberg Drift

Previous studies [Gladstone *et al.*, 2001; Silva *et al.*, 2006] discussed the difference in drift between smaller and larger icebergs, with the overall result that larger icebergs tend to stay in the westward coastal current around Antarctica while smaller icebergs show a northward drift component early in their lives. This dependence can be clearly seen in our simulation including giant icebergs (Figure 2, left): as a rule of thumb, smaller icebergs (blue trajectories) tend to spread toward the open ocean all around Antarctica. In contrast, giant icebergs (magenta trajectories) stay close to the Antarctic coast in most cases and leave it only at well-defined separation points in the Weddell Sea, the Ross Sea, and near the Kerguelen Plateau, from where they can travel to lower latitudes beyond 50°S.

From the momentum balance in equation (1), it is immediately clear that the relative importance of the different driving forces depends on iceberg mass and size: only the body forces (Coriolis and surface slope) are proportional to the iceberg mass, so that those forces become increasingly important for larger icebergs (Figure 3). For giant icebergs, in the absence of sea ice, the momentum balance is mainly between Coriolis and the sea surface slope, resulting in iceberg velocities close to the geostrophic ocean velocity, so that  $F_o \approx 0$ . It is thus very difficult for giant icebergs to cross isolines of sea surface height (SSH) and to leave the coastal current. Since the force due

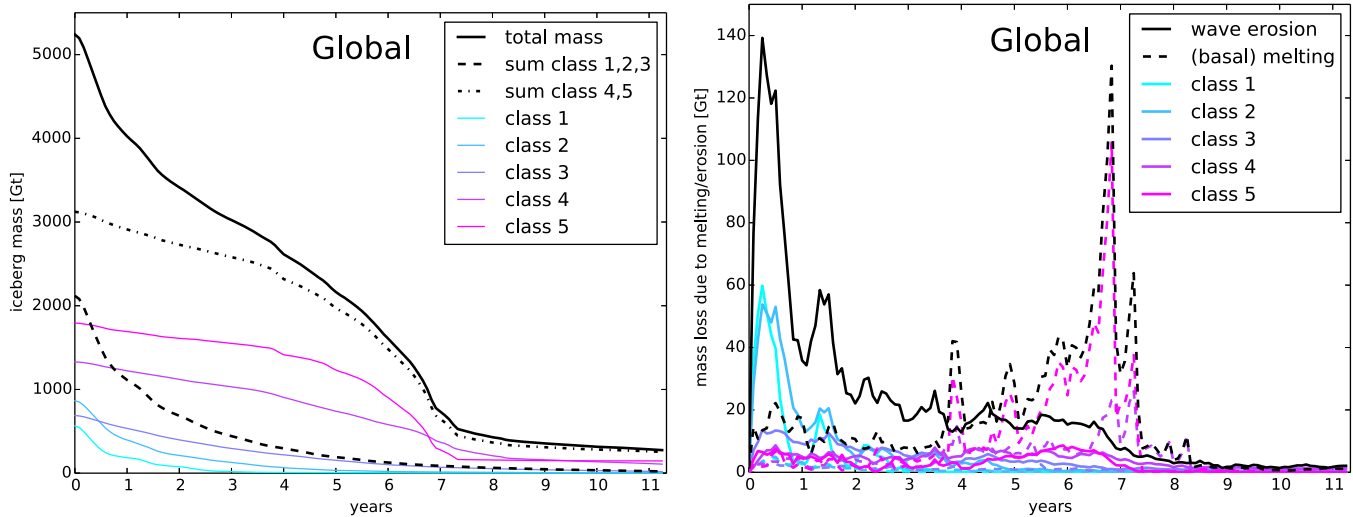


**Figure 4.** (left) Time series of the iceberg mass. The total mass (black line) is split into the summed mass of icebergs initially classified as “small-to-medium” (classes C1–C3, dashed line) and as “giant” (classes C4 and C5, dashed-dotted line). The total mass in every single class defined by *Wesche and Dierking* [2015] is also given (colored lines). (right) Time series for the mass input due to melting and wave erosion. Wave erosion (black solid line) and basal melting (black dashed line) are also given for every single class (colored solid and dashed lines). Being of smaller value, the other melt rates (buoyant convection and “basal” lateral melting) have been included in the “(basal) melting” term.

(Figure 4, left). In order to highlight the effect of initial iceberg size, icebergs do not change size class in our analysis despite shrinking due to melting, i.e., icebergs initially classified as giant icebergs will stay in classes C4 and C5.

The global time series of iceberg mass shows two regimes: First, there is an exponential decay of mass within the first 4 years after initialization. Subsequently, there is a second period of accelerated decay lasting for 3 years, during which the iceberg mass diminishes rapidly. Ten years after initialization, basically all icebergs have melted and only some mass is left from icebergs initially classified as giant icebergs (classes C4 and C5).

The behavior in the first regime can be explained by the exponential decay of the mass of small and medium-sized icebergs in classes C1–C3, with a mean lifetime of  $\tau \approx 2$  years. This is largely due to wave erosion at the sides (Figure 4, right). In contrast, the mass of initially giant icebergs in classes C4 and C5 decreases very slowly in the first 4 years. It is only between year 4 and 5 after initialization that the mass of those icebergs starts to diminish faster, continuing for about 3 years. The timing of increased decay of giant icebergs coincides with the time when those icebergs reach lower latitudes with warmer ocean waters. Consequently, their reduction in size is then mainly due to basal melting at the bottom (Figure 4, right), indicated by the shift of importance from wave erosion to basal melting in the second half of the fourth year. Specifically, the two largest giant icebergs in the simulation leave the coastal current near the Kerguelen Plateau between 60°E and 90°E (see, e.g., magenta lines in Figure 2, left). Being captured by the expanding sea ice, they both cross the southern ACC front [*Orsi et al.*, 1995] around July with increased velocities relative to the ocean due to the fact that sea ice drift speed is generally larger than ocean current velocities. The combination of this dynamical effect and the warmer waters northward of the front leads to a rapid increase of basal melt rates, which reduce again to lower levels after the influence of the sea ice has ceased. However, while basal melting and wave erosion had been of similar magnitude prior to crossing the front, basal melting remains the dominant mechanism thereafter.

#### 4. Climatological Iceberg Freshwater Input Estimates

Estimates for the freshwater input from melting icebergs are of particular interest, not only to the ocean modeling community. In a balanced state, the climatological iceberg mass input to the ocean per unit time equals the climatological calving rate of the Antarctic ice sheet, estimated as  $1321 \pm 144$  Gt per year by *Depoorter et al.* [2013]. Iceberg calving is therefore of the same importance for the mass balance of the Antarctic ice sheet as estimated ice-shelf melting ( $1454 \pm 174$  Gt per year) [*Depoorter et al.*, 2013]. More than a decade before, *Gladstone et al.* [2001] already determined a climatological calving rate of 1332 Gt per year,

which is very close to the estimate by *Depoorter et al.* [2013]. The spatial and temporal distribution of the freshwater from melting icebergs is, however, still insufficiently constrained.

#### 4.1. Previous Estimates

An annual-mean climatological estimate of iceberg melt has been presented by *Silva et al.* [2006]. They determined melt rates along observed tracks of giant icebergs and combined the resulting melt pattern with simulation results by *Gladstone et al.* [2001] for small icebergs of up to 2.2 km in size. A very recent study by *Merino et al.* [2016] produced an updated version of the *Gladstone et al.* [2001] data set. They applied the calving fluxes for Antarctic icebergs by *Depoorter et al.* [2013] within the NEMO ocean modeling framework, with an iceberg model (*Marsh et al.* [2015] based on *Martin and Adcroft* [2010]) very similar to the *Gladstone et al.* [2001] study, again modeling icebergs only up to sizes of 2.2 km and neglecting larger icebergs. One drawback of this method is the fact that the climatological calving fluxes integrate the contributions from very different iceberg size classes, ranging from regularly calving small icebergs to giant tabular icebergs that only calve on decadal timescales; however, the whole flux is effectively used for the evolution of small icebergs only. Since drift and melt depend on the iceberg size (see sections 3.3 and 3.4), the resulting melt pattern is systematically biased toward the pattern associated with smaller icebergs.

#### 4.2. Estimation of Climatologies From the FESOM-IB Simulation

The few available estimates of climatological iceberg meltwater input are mostly model-based. It is hence very important to compare different estimates with each other and to identify similarities and differences. We use the simulated small to giant iceberg trajectories and along-track melt rates from FESOM-IB to produce a set of monthly iceberg melt climatology estimates. Since our simulation resembles an initial value problem (instead of a boundary problem with prescribed calving fluxes), our chosen methodology to estimate iceberg melt climatologies demands separate clarification (see below). To put those estimates into perspective, we compare the magnitude of the freshwater input from melting icebergs to sea ice production/melting rates as well as to the difference of precipitation and evaporation (P-E) over the Southern Ocean (section 4.3), and to data from the study by *Merino et al.* [2016] (section 4.4).

To facilitate the comparison with the study by *Merino et al.* [2016] and in order to estimate the effect of including larger icebergs into the climatology, we produce four iceberg melt climatologies, based on four size classes with increasing maximum size limit (see definition in Figure 1, right columns). The classes comprise (1) “small” icebergs up to 2.2 km length (“SMA”), following previous studies; (2) “small-to-medium-sized” icebergs from classes C1 and C2 (“MED12”); (3) “small-to-medium-sized” icebergs from classes C1–C3 (“MED123”); and (4) “small-to-giant-sized” icebergs (class “ALL”).

For every class, we compute a monthly sum of melt rates based on the entire simulation. Afterward, the monthly patterns are scaled so that the total freshwater input is 1321 Gt per year, as suggested by *Depoorter et al.* [2013]. In detail, the along-track melt rates are accumulated both month-wise (for January to December) and spatially for every grid box of a regular  $1^\circ \times 1^\circ$  lat-lon grid. This yields some intermediate “climatological” patterns  $M_k$ , where  $k = 1, \dots, 12$  denotes the month. Using the “ALL” class as an example, its total mass input amounts to  $\|M\|_a \approx 5000$  Gt (the melted iceberg mass in 12 years of simulation), where  $\|\cdot\|_a$  denotes the integrated annual-mean freshwater input. To ensure an integrated freshwater input of 1321 Gt per year as suggested by *Depoorter et al.* [2013],  $M$  is then scaled down to obtain a monthly melt climatology estimate

$$M_{\text{clim},k} := M_k / \|M\|_a \times 1321, \quad k = 1, \dots, 12 \quad (8)$$

An analogous computation is performed for the MED123 ( $\|M\|_a = 2100$  Gt), MED12 ( $\|M\|_a = 1430$  Gt), and SMA ( $\|M\|_a = 1076$  Gt) classes. We note that when taking successively larger icebergs into account (the maximum size limit increases when going from SMA to ALL), scaling ensures that the weight of smaller icebergs in the pattern is successively decreased because a total mass input of 1321 Gt per year is guaranteed in all climatology estimates.

The annual-mean melt patterns from the four climatology estimates are shown in Figure 5. Typical values around the coast lie between 0.1 and 1 mm d<sup>-1</sup>, with values reaching as high as 10 mm d<sup>-1</sup> in large parts of the Indian Ocean sector, which is mainly due to erosion from surface waves (not shown). In all sectors, including larger icebergs leads to the inclusion of successively longer trajectories and higher meltwater

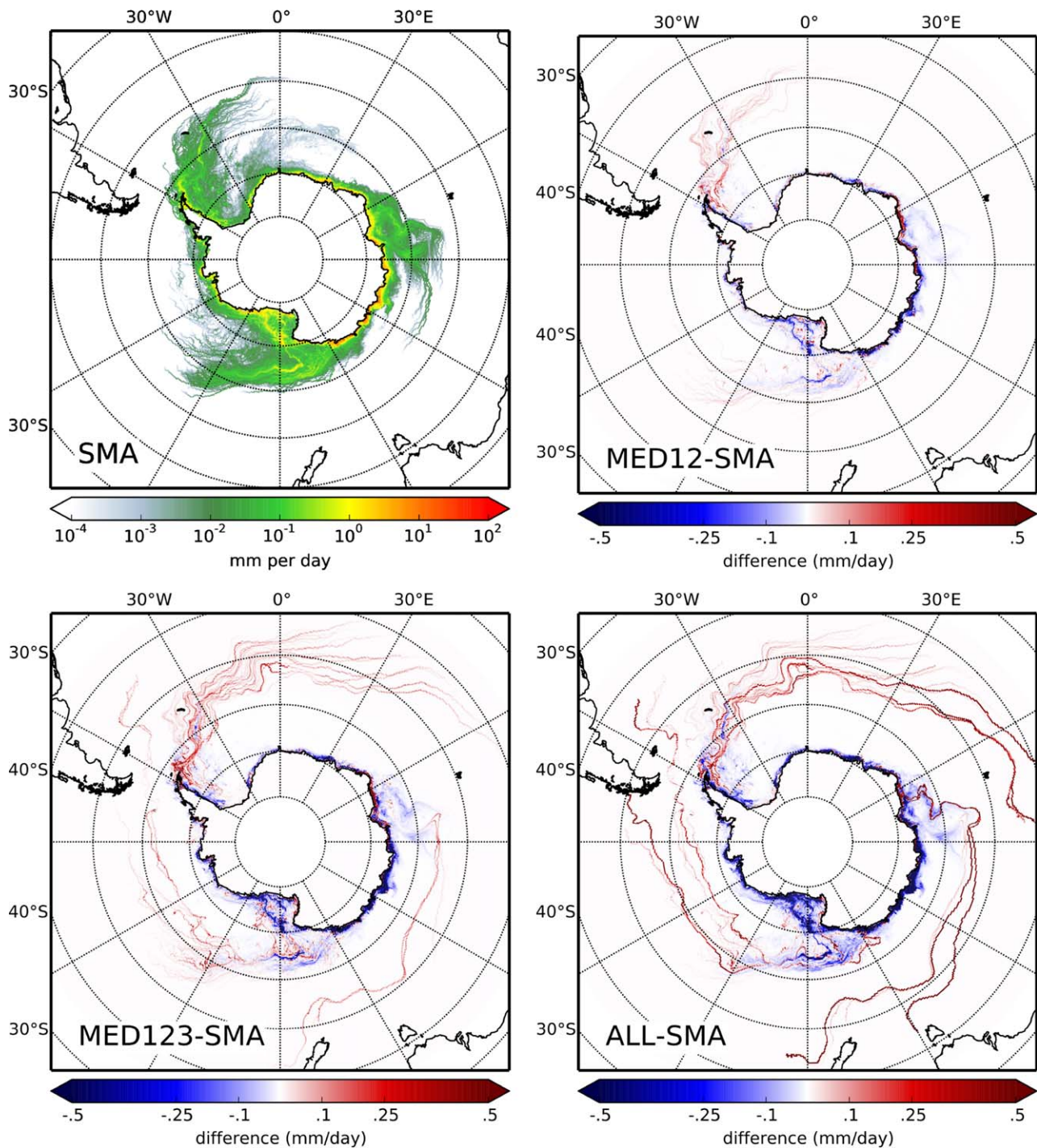


**Figure 5.** Iceberg meltwater climatology estimates [ $\text{mm d}^{-1}$ ] based on four different size classes. The modeled trajectories and along-track melt rates have been accumulated on a  $0.25^\circ$  regular lon-lat grid (for the rest of this study a  $1^\circ$  regular lon-lat grid is used). (top left) Meltwater climatology based on small icebergs up to 2.2 km in size (SMA). (top right) Difference between the meltwater climatology based on size classes C1 and C2 and the meltwater climatology based on small icebergs (MED12-SMA). (bottom left/right) Same as top right, but for size classes C1–C3 (MED123-SMA), and for all trajectories (small-to-giant) from classes C1–C5 (ALL-SMA). All climatologies have been scaled to the same integrated input of 1321 Gt/yr.

input at lower latitudes. Correspondingly, the relative meltwater input along the coast, especially in the Indian Ocean sector, decreases. The generally increasing northward mass transport with increasing maximum size limit for the windmill-like branches is studied in more detail in section 4.4.2. Conversely, accounting for larger icebergs leads to successively smaller meltwater input within the second (eastern) branch in the Weddell Sea that is only followed by smaller icebergs.

4.3. Relative Importance Compared to P-E and Sea Ice Production Rates

In order to put the freshwater input from melting icebergs into perspective, we compare its magnitude to the difference between precipitation and evaporation (P-E) over the Southern Ocean, where P-E is mainly positive (Figure 6, top left). The magnitude of the meltwater input is on the order of 5–20% of the P-E balance in large areas of the Southern Ocean (Figure 6, bottom left), with local maxima exceeding P-E. In coastal areas, the freshwater input is generally larger than 20% of P-E in all climatology estimates and therefore of the same order of magnitude.

Melting (production) of sea ice is also associated with positive (negative) freshwater fluxes (Figure 6, top right). The freshwater flux from melting icebergs is on the order of 5–20% of coastal sea ice production rates (Figure 6, bottom right), but with different sign, and opposes the effect of brine rejection to the ocean in the annual mean. Along the sea ice edge, the freshwater flux from iceberg melting amounts to more than 20% of the freshwater flux associated with sea ice melting. Naturally, this is also the case in the area to the north of 50°S where no sea ice is found (60°S in the Pacific sector), making iceberg melting the largest vector of freshwater flux from frozen ice northward of these latitudes.

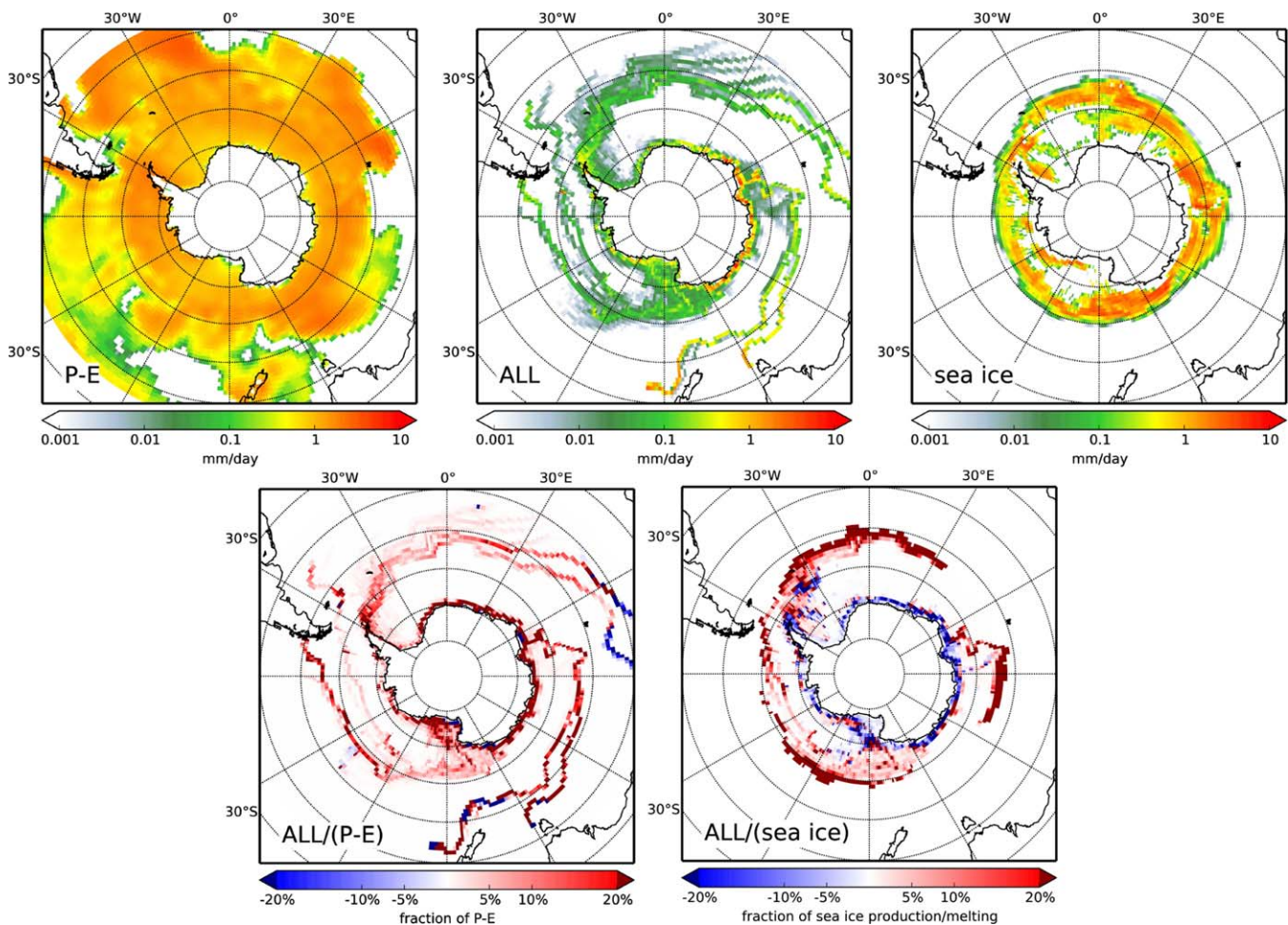


**Figure 6.** Annual-mean freshwater input [ $\text{mm d}^{-1}$ ] due to iceberg melting in the Southern Ocean in relation to precipitation minus evaporation (P-E) and sea ice production/melting. (top middle) Iceberg meltwater input in the ALL climatology estimate. (top left) Mean freshwater flux from P-E and (top right) from sea ice melting in  $1^\circ \times 1^\circ$  grid boxes from the FESOM-IB simulation with CORE.v2 forcing [Large and Yeager, 2009] for the period 1997–2008. For P-E, white areas indicate a balance below  $10^{-3} \text{ mm d}^{-1}$ , including negative values; for sea ice, white areas inside the area enclosed by sea ice indicate regions of sea ice production. (bottom left) Iceberg meltwater input in percentage of P-E for the ALL climatology estimate [ALL/(P-E)]. Dark red areas indicate grid boxes where the meltwater input is at least of the same order as P-E, according to the criterion “meltwater  $> 0.2(\text{P-E})$ ” from [Silva et al., 2006, Figure 6]. (bottom right) Same as bottom left, but for sea ice production/melting [ALL/(sea ice)]. Dark blue areas indicate grid boxes where the meltwater input is at least of the same order as sea ice production, with different sign.

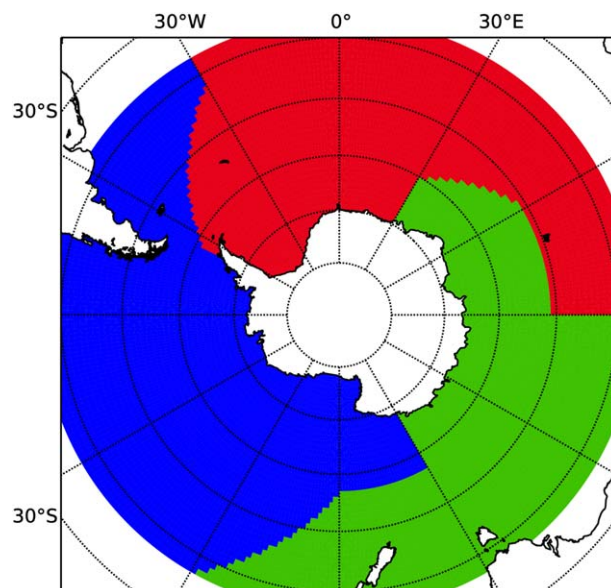


**Figure 7.** Definition of the sectors used in this study: Atlantic Ocean (red; 64°W–30°E), Indian Ocean (green; 30°E–150°E), and Pacific Ocean (blue, 150°E–64°W). The coastal definition of the sectors is modified at lower latitudes, following the windmill-like northward reaching branches of the iceberg trajectories, in order to evaluate the northward transport of mass in the different branches (section 4.4.2).

#### 4.4. Comparison With Another Climatology

To identify common characteristics as well as differences, we compare the four climatology estimates with the NEMO climatology of *Merino et al.* [2016], which is based on small icebergs up to 2.2 km length (identical to the SMA class). Given that the FESOM-IB estimates have been scaled to an annual-mean meltwater input of 1321 Gt per year, we can now directly compare with the results by *Merino et al.* [2016]; they used the calving fluxes by *Depoorter et al.* [2013] as boundary conditions, amounting to the same value.

The comparison is done between the Atlantic, Pacific, and Indian Ocean sectors (for a definition of the sectors, see Figure 7). In the case of FESOM-IB, we note that the bulk of the initial iceberg mass (70%) as determined by *Wesche and Dierking* [2015] for September/October 1997 is concentrated in the Indian Ocean, and only 20% (10%) is located in the

Pacific (Atlantic). It is unclear whether the specific weighting in 1997 between the sectors is generally valid, or whether it is a result of interannual variability in calving or drift-related variability, or a combination of both. It might also, at least partly, be explained by the slight coverage bias in the *Wesche and Dierking* [2015] data set (section 2.4.1).

Compared to the NEMO climatology (Figure 8), the total amount of freshwater that enters the Pacific sector is similar in the FESOM-IB estimates (257–389 Gt; NEMO: 355 Gt). While the shape of the drift pattern is also similar, the trajectories in the Ross Sea are slightly shifted between NEMO and FESOM-IB. Considering the observed trajectories in the Ross Sea from the BYU database (Figure 2, right), the more westerly trajectories simulated with FESOM-IB appear to be more realistic.

A large difference can be found in the northwestern Weddell Sea along the Antarctic Peninsula and around (and in the lee of) the South Orkney Islands. The total amount of freshwater that enters the Atlantic sector is more than 2 times higher in NEMO (589 Gt) than in FESOM-IB (153–245 Gt). In turn, the Indian Ocean mass input amounts to 785–818 Gt in FESOM-IB and to only 380 Gt in NEMO. We hypothesize that this can mainly be attributed to the different treatment how icebergs are initialized in the models, and the particular relative initial mass weighting in 1997 as given by the *Wesche and Dierking* [2015] data set (see also discussion in section 2.4).

The difference pattern between the FESOM-IB estimates and NEMO in the Weddell Sea shows a bifurcation into two separate branches, extending north and south of the South Orkney Islands. We note that the iceberg code by *Merino et al.* [2016] is based on the formulation of *Martin and Adcroft* [2010], who introduced “bergy bits” to their simulation (child icebergs formed from wave erosion that are assumed to travel with their parent iceberg). This effectively delays the input of iceberg meltwater to the ocean. Thus, more meltwater enters the ocean at the northern edge of the Weddell Sea, leading effectively to somewhat increased northward freshwater transport in the Weddell Sea [*Martin and Adcroft*, 2010], even without considering larger icebergs. Accordingly, the difference pattern between the FESOM-IB and NEMO estimates in the Weddell Sea resembles the difference pattern between their simulations with and without “bergy bits” [*Martin and Adcroft*, 2010, Figure 3].

Including larger icebergs in the FESOM-IB estimates leads to an inclusion of successively longer trajectories in all sectors, associated with higher meltwater input at lower latitudes (Figure 8, bottom right). This is

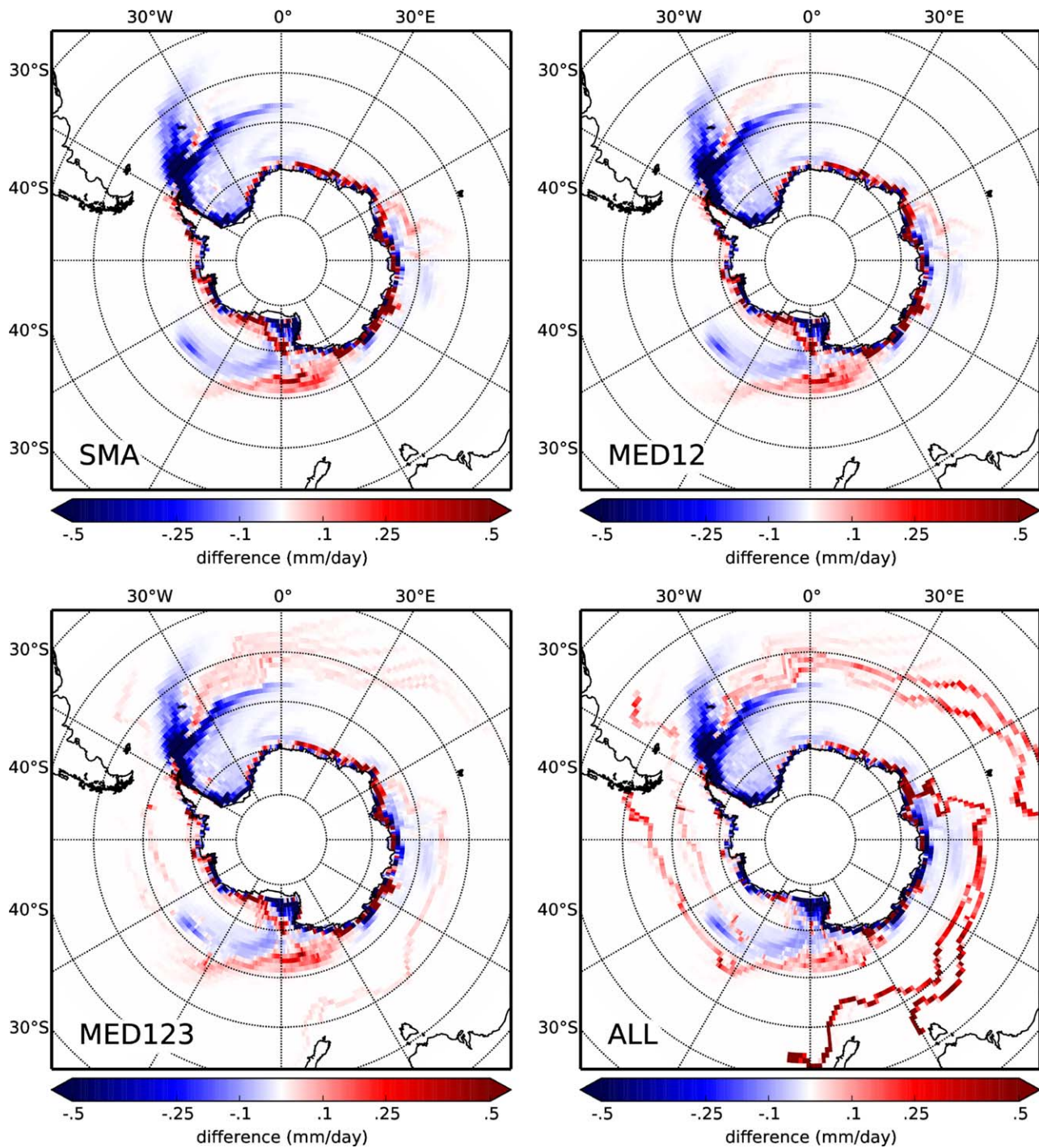
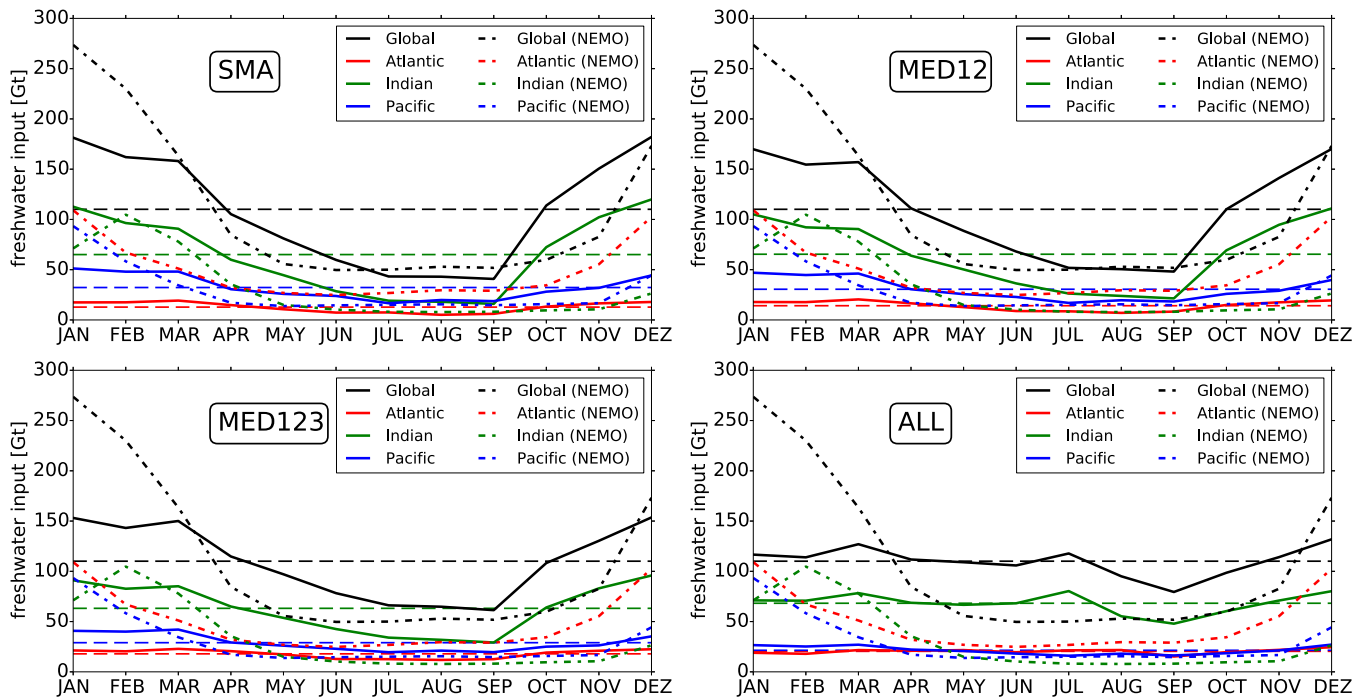


Figure 8. Annual mean difference (FESOM-NEMO, in  $\text{mm d}^{-1}$ ) for the four FESOM-based iceberg meltwater climatologies relative to NEMO-based estimates from Merino *et al.* [2016].

studied quantitatively in section 4.4.2, where zonal sums of iceberg melt are compared to the NEMO estimate. Interestingly, the successively longer trajectories in the Weddell Sea mainly pass through the middle of the scissors-like bifurcation mentioned before, meaning that icebergs in NEMO tend to travel either to the north or south of the FESOM-IB trajectories after passing the tip of the Antarctic Peninsula.

#### 4.4.1. Seasonality

The FESOM-IB SMA estimate shows a strong seasonality of iceberg melting (Figure 9, top left), which is also evident in the NEMO climatology of Merino *et al.* [2016]. While the individual seasonal cycles in the Atlantic,



**Figure 9.** Seasonal cycle of freshwater input [Gt/month] for the four climatologies based on different size classes. (top left) Small icebergs up to 2.2 km side length (SMA), (top right) small-to-medium icebergs from classes C1 and C2 (MED12), (bottom left) small-to-medium icebergs from classes C1–C3 (MED123), and (bottom right) small-to-giant icebergs from classes C1–C5 (ALL). Horizontal dashed lines depict the annual mean input; the seasonal cycle from the NEMO climatology by Merino *et al.* [2016] is shown for comparison (dashed-dotted lines).

Indian Ocean, and Pacific Ocean sectors show some differences between the model setups, the global seasonal cycle is very similar concerning the timing of the minimal and maximal freshwater input. The seasonality is linked to the strong seasonality of the integrated Antarctic sea ice area, which strongly damps the wave erosion in austral winter when sea ice concentrations are high. The higher freshwater input in October (and November) in the FESOM-IB estimate relative to the NEMO climatology is partly attributable to the chosen initialization in 29 September 1997, leading to the largest iceberg mass available for melting in the following 2 months. Since only  $\sim 25\%$  of the initial iceberg mass melts within the first year (Figure 4, left), the monthly meltwater flux is, however, only slightly biased toward the end of the year.

Interestingly, the seasonality successively decreases when larger icebergs are included into the climatology estimates. This can be explained by the increasing (decreasing) importance of basal melting (wave erosion) for larger icebergs (Figure 4, right). Wave erosion and the lateral melt terms are all proportional to the area of an iceberg's sidewall  $LH$  (with draft  $D \approx H$ ), while basal melting is proportional to the bottom area of an iceberg,  $L^2$  (section 2.3.3). The ratio between  $L^2$  and the areas the lateral decay terms are acting on is thus proportional to  $L/H$ . Considering variations of the surface area, basal melting will therefore increase for larger icebergs because  $L/H \gg 1$ .

Moreover, larger icebergs that reach the ACC with its warmer waters erode far away from the sea ice edge and its strong seasonality. Particularly, when giant icebergs are included in the ALL estimate, the seasonality is strongly reduced and virtually absent (Figure 9, bottom right). This is in stark contrast to the findings by Merino *et al.* [2016] for small icebergs, and an important argument for the inclusion of giant icebergs into meltwater estimates.

#### 4.4.2. Sector-Wise Mass Input as Function of Latitude

In this section, we analyze the sector-wise meridional distribution of the initial iceberg mass as a function of latitude for the four climatologies with FESOM-IB and for the NEMO climatology by Merino *et al.* [2016]. The global mass input is significantly altered with successive inclusion of larger icebergs, resulting in a larger mass input at lower latitudes (Figure 10). To quantify this further, we compute the mass input to the north of  $58^\circ\text{S}$ . This is approximately the latitude where the zonally summed global mass input features a local minimum for the ALL climatology (Figure 10, top left). This latitude is thus particularly suitable to

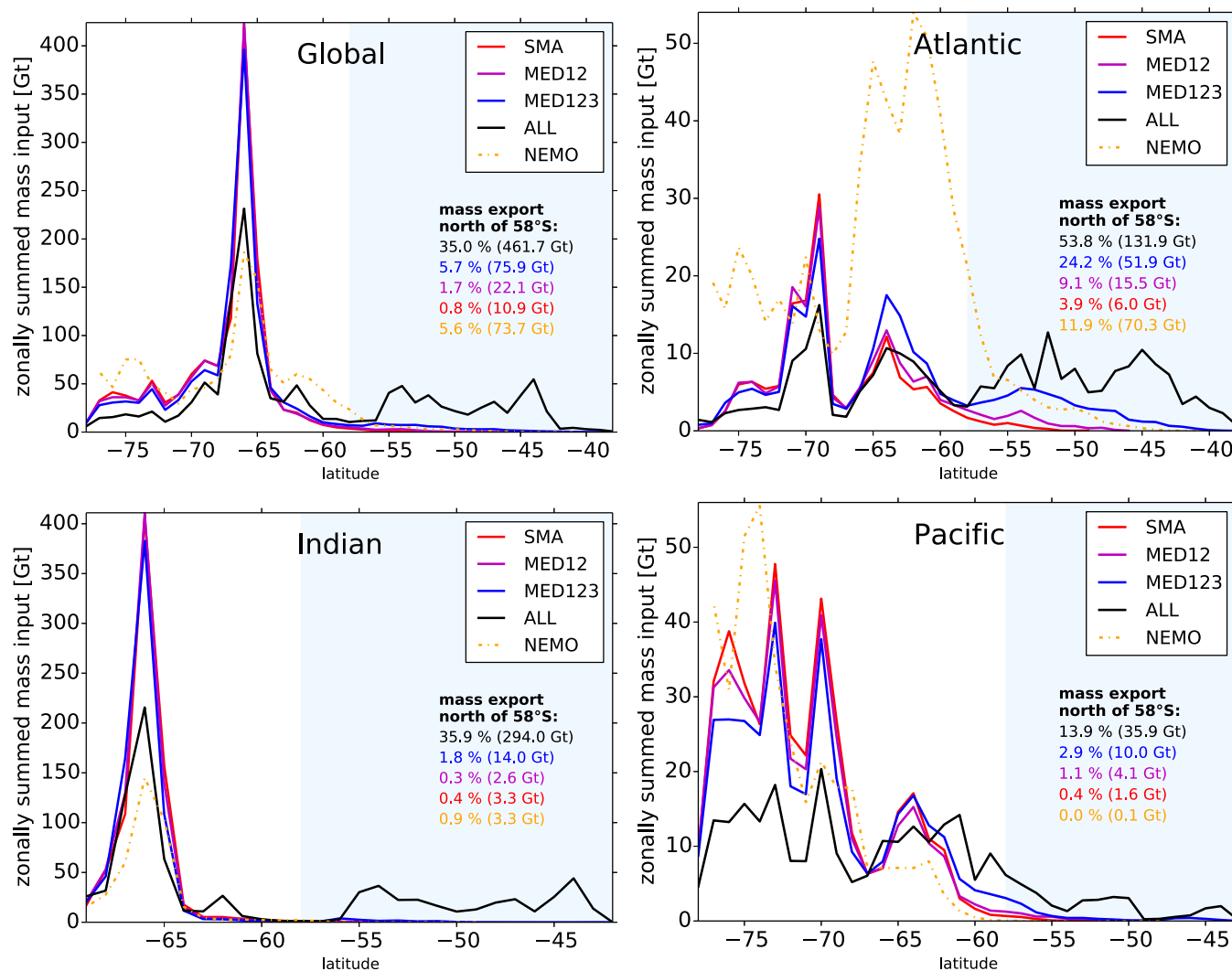


**Figure 10.** Zonally summed mass input [Gt] for the different climatology estimates as a function of latitude ( $1^\circ$  spacing) for (top left) the whole Southern Ocean, (top right) the Atlantic sector, (bottom left) the Indian Ocean sector, and for (bottom right) the Pacific sector. Blue shading indicates the area to the north of  $58^\circ\text{S}$ ; the corresponding mass export is given in %. Dashed yellow lines show the zonally summed mass input from the NEMO climatology by Merino *et al.* [2016] for comparison.

illustrate the very different mass transports to lower latitudes in the climatology estimates. Since the previous section revealed differences between the model setups in terms of the total mass input in the different sectors, we also discuss percental values to facilitate the comparison.

Globally, 35% of the mass of icebergs is exported to the area north of  $58^\circ\text{S}$  in the ALL climatology, largely due to the inclusion of giant icebergs (Figure 10, top left). In the climatology considering solely small icebergs up to sizes of 2.2 km (SMA), only 0.8% of the iceberg mass is exported to the north of this latitude. The value for the NEMO climatology (5.6%) is significantly lower than the FESOM-IB ALL estimate, but larger than the SMA estimate, possibly due to the inclusion of “bergy bits” in the simulation by Merino *et al.* [2016] and its apparently strong impact in the Weddell Sea. As a result, their global mass export across  $58^\circ\text{S}$ , based on small icebergs, is almost identical to our MED123 estimate (5.7%), which already includes icebergs up to sizes of  $100\text{ km}^2$ .

Sector-wise, large differences between the FESOM-IB ALL and NEMO transports across  $58^\circ\text{S}$  are apparent in the Indian and Pacific Oceans (Figure 10, bottom). Here the NEMO climatology features very little transport across  $58^\circ\text{S}$  (0–0.9%) compared to values of 35.9% (Indian) and 13.9% (Pacific) in the FESOM-IB ALL estimate. This is primarily due to the inclusion of giant icebergs from size classes C4–C5, since the MED123 transports are still only 1.8 and 2.9%, respectively. Another large difference between the models can be

found in the Atlantic sector, where NEMO features a broad maximum of freshwater input to the south of 58°S (Figure 10, top right). As mentioned before, we hypothesize that the absolute difference between the models in the Weddell Sea can mainly be attributed to the different treatment how icebergs are initialized, and the particular relative initial mass weighting in 1997 as given by the *Wesche and Dierking* [2015] data set (see discussion in section 2.4). However, even though the total mass input into the Atlantic is more than 2 times higher in the NEMO climatology (see section 4.4), the total mass transport across 58°S in FESOM-IB ALL is about twice (131.9 Gt) as large as in NEMO (70.3 Gt), because 53.8% of the Atlantic iceberg mass in ALL is exported across this latitude compared to only 11.9% in the NEMO climatology.

*Silva et al.* [2006] estimated that, globally, 35% of the mass of giant icebergs is exported across 63°S, while only 3% of the mass of small icebergs reach those latitudes. While the first estimate is based on observed iceberg tracks and their modeled melt rates, the latter estimate is based on the model results by *Gladstone et al.* [2001] (without “berg bits”). Therefore, we also computed the mass export across 63°S in FESOM-IB and in the NEMO climatology. The *Silva et al.* [2006] estimate supports our results with FESOM-IB: the mass transport to lower latitudes than 63°S successively increases from 6% (SMA) and 6.9% (MED12), over 12.5% (MED123), to an export as high as 45% (ALL) when giant icebergs are included. Compared to its low export across 58°S, the NEMO estimate has a relatively high export across 63°S (23.6%) even without medium-sized icebergs—ranging between the FESOM-IB estimates for medium-sized and for small-to-giant icebergs.

## 5. Discussion and Conclusions

We present a simulation of Antarctic iceberg drift and melting that includes small, medium-sized, and giant tabular icebergs with a realistic size distribution. For the first time, an iceberg model is initialized with a set of nearly 7000 observed iceberg positions and sizes around Antarctica. The study highlights the necessity to account for large icebergs in order to obtain accurate melt climatologies. Future ocean simulations will benefit from an improved meridional distribution of iceberg melt, especially in climate change scenarios where the impact of iceberg melt is likely to increase due to increased calving from the Antarctic ice sheet.

Our model is initialized with instantaneous near-coastal iceberg conditions from September 1997 and reproduces typical drift patterns for a large spectrum of size classes. The magnitude of the associated meltwater input is generally on the order of 5–20% of the P-E balance in large areas of the Southern Ocean, especially around the coast, with local maxima even exceeding P-E. Furthermore, the freshwater flux from melting icebergs is on the order of 5–20% of coastal sea ice production rates and, thus, partly compensates the effect of brine rejection in the annual mean. Iceberg melting is the largest vector of freshwater input from frozen ice along (and northward of) the sea ice edge.

Our results indicate that basing the meltwater climatology estimate on small icebergs (up to 2.2 km side lengths) results in the majority of freshwater entering more near-coastal areas as also found in another recent meltwater estimate [*Merino et al.*, 2016]. In contrast, estimates including medium-sized and giant icebergs result in more freshwater reaching lower latitudes, even regions northward of 58°S. A strong seasonality caused by lateral erosion from surface waves is found in our simulation for small icebergs only, similar to what was shown by *Merino et al.* [2016]. However, the seasonality strongly decreases with the inclusion of larger icebergs and is virtually nonexistent when giant icebergs are considered as these erode mostly due to bottom melt. The inclusion of giant icebergs into the melt climatology thus leads to strong changes compared to estimates based on small icebergs only. The “berg bits” parameterization in the NEMO code apparently compensates for some of this difference, particularly in the Weddell Sea.

Throughout the paper, we use the term “climatology estimate” because FESOM-IB is initialized with instantaneous conditions from September/October 1997, which might be subject to seasonal and interannual variability, and episodically calving giant icebergs will be distributed differently between the years. Although the model is run for 12 years, the variability of drift tracks is thus potentially biased to the chosen initialization. As a result, the climatology estimates including larger icebergs are less smooth than what might be expected from a climatology. In particular, single trajectories can be identified for the rare giant icebergs, posing a statistical challenge [*Stern et al.*, 2016]. Single trajectories and the resulting meltwater pattern of giant icebergs could only be smoothed by averaging over several hundreds of years, since both calving and melting takes place on decadal timescales. In that sense, the climatology estimate including giant icebergs

has to be regarded as one particular realization of giant icebergs' drift and decay, being representative for the decade following 1997 rather than general present-day climate. Starting the simulation from several different ocean states and running it through different decades of atmospheric forcing could yield an ensemble-based error estimate for the computed meltwater climatology.

We want to stress that a smoother melt climatology, taken over several hundreds of years, would lack the strong local peaks by giant icebergs, which are constantly observed around Antarctica. In other words, the real meltwater pattern in any particular year arguably resembles our climatology estimate for giant icebergs more closely than it would resemble a smoothed version of it, with the exception that giant iceberg trajectories will differ between individual years in northward extent, length, and number. Keeping this in mind, we consider a climatology for giant icebergs like the one presented in this study highly relevant for a number of conceivable studies, e.g., biogeochemical process studies or sensitivity experiments of the oceanic response to the meltwater input from giant icebergs.

We did not attempt to find optimal model parameters and drag coefficients for the different size classes. To allow for a stringent optimization of model parameters, a linear relationship between drag coefficients and iceberg mass could be implemented in future versions of the model as shown by *Keghouche et al.* [2009] for Arctic icebergs. Moreover, although the model includes the established iceberg physics, several mechanisms are not implemented yet that could potentially influence (giant) iceberg drift. A parameterization for the breakup of icebergs into smaller bits that goes beyond the parameterization of wave erosion is missing [*Stern et al.*, 2016]. Such a parameterization would supposedly affect the length of iceberg trajectories in the warm waters of the ACC rather than the meridional distribution of iceberg mass as determined in this study. Furthermore, additional physical mechanisms not considered so far include a parameterization of possible Taylor-Proudman columns below giant icebergs with very deep drafts [*Crépon et al.*, 1988], and the effect of atmospheric pressure gradients on giant icebergs, potentially important in iceberg "graveyards" or "parking lots" [*Turnbull*, 2010].

Future versions of FESOM-IB will aim for a two-way coupling of iceberg meltwater and heat fluxes (sensible and latent) to the ocean, allowing for the study of iceberg-related feedbacks. We expect that a coupling of three-dimensional melt fields to the ocean hydrography could strongly affect the vertical structure of the upper water column, with potential effects on the melt fields themselves. In combination with the biogeochemical module for FESOM [*Schourup-Kristensen et al.*, 2014], another important field of research could be tackled quantitatively, e.g., the impact of iron fertilization by icebergs on biological productivity and the associated sequestration of atmospheric CO<sub>2</sub> [*Arrigo et al.*, 2008].

*Stern et al.* [2016] summarize three challenges for the inclusion of giant icebergs into model simulations, which we already address to some degree in this study. The first challenge is of numerical type and relates to the possible violation of the Lagrangian point assumption, which we partly mended here by averaging the sea surface slope over surrounding model grid elements; moreover, in order to force the model, we use (1) in situ temperature and salinity values at the iceberg bottom for processes related to basal melting and (2) averages from vertical profiles of ocean currents, temperature, and salinity instead of only their surface representation for all lateral processes. Second, calving of giant icebergs is limited to specific regions [*Wesche et al.*, 2013], so *Stern et al.* [2016] argue that models prescribing calving rates would need spatially variable calving distributions, which is not an issue in our model. Their important last concern relates to the inclusion of giant icebergs, since those would make climate simulations dependent on statistically rare events. In contrast to potential fully coupled earth system model setups, the ocean does not respond to the iceberg melt from giant icebergs in our specific setup. Only the sensitivity of the meltwater pattern to the inclusion of larger icebergs is studied; the dependence of the ocean on these rare events and possible feedbacks, however, still need to be quantified in future studies. A possible way around the statistical concern raised by *Stern et al.* [2016] would be to *not* simulate giant icebergs in coupled earth system models interactively at all; instead, one could perform ocean-only simulations with one-way coupling as in this study over hundreds of years for different starting years and initial conditions, and just use the averaged melt patterns as spatiotemporal templates for the redistribution of calved land-ice over the ocean in climate models. That way the typical meridional distribution of giant iceberg melt would be retained without any dependence on statistically rare events. However, we wish to stress that single calving events of giant icebergs could be relevant to ocean dynamics and biogeochemistry, similar to the important role of single volcano eruptions in historical simulations of climate.

To summarize, we have shown that the inclusion of successively larger icebergs strongly changes the meridional distribution of the meltwater input to the ocean as well as its seasonality. This study highlights the importance of giant icebergs and systematic shortcomings of previous meltwater estimates. We, therefore, propose that iceberg modeling research should focus on the issue of how best to include giant icebergs into climate simulations.

The four melt climatology estimates presented in this study are freely available [Rackow *et al.*, 2016b] and can be used for sensitivity studies with uncoupled models to investigate the response of the ocean and sea ice. In addition, the normalized melt patterns can be used in CMIP-type climate models like the AWI Climate Model [Sidorenko *et al.*, 2015; Rackow *et al.*, 2016a] to close their water cycle: snow over the Antarctic ice sheet is often not accumulated in the absence of an interactive ice sheet model; instead, it is treated as excess freshwater and arbitrarily transported to the ocean, with varying solutions between models [Martin and Adcroft, 2010]. Instead of choosing a global redistribution or a treatment as coastal Antarctic runoff, the normalized melt patterns can be utilized for the redistribution of the excess freshwater over the Southern Ocean, away from the coastal regions. While the estimate based on small icebergs (“SMA”) can be considered to be a more conservative estimate for that purpose in line with previous studies, only the “ALL” estimate comprises giant icebergs and shows the strongest changes compared to previous estimates. The Year of Polar Prediction, with its core phase from mid-2017 through mid-2019, offers a unique opportunity for intense iceberg observations [Jung *et al.*, 2016], and more data similar to the *Wesche and Dierking* [2015] data set with higher spatial and temporal coverage should be acquired to reduce the uncertainty of future iceberg melt climatologies.

#### Acknowledgments

The  $1^\circ \times 1^\circ$  melt climatology estimates for the different size classes are available at the PANGAEA website (<https://doi.org/10.1594/PANGAEA.865335>). Higher resolution versions (e.g.,  $0.25^\circ \times 0.25^\circ$ ) and the raw trajectories for the 6912 icebergs can be made available upon request to [thomas.rackow@awi.de](mailto:thomas.rackow@awi.de). We thank Dmitry Sidorenko, Sergey Danilov, Qiang Wang, Helge F. Goessling, and Jens Schröter for helpful discussions. Madlen Kimmritz and Nils Hutter significantly accelerated the writing and postprocessing of the trajectory output. Computational resources were made available by the North-German Supercomputing Alliance (HLRN). Comments and suggestions of two anonymous reviewers are greatly acknowledged.

#### References

- Arrigo, K. R., G. van Dijken, and M. Long (2008), Coastal Southern Ocean: A strong anthropogenic CO<sub>2</sub> sink, *Geophys. Res. Lett.*, *35*, L21602, doi:10.1029/2008GL035624.
- Bigg, G. R., and D. J. Wilton (2014), Iceberg risk in the Titanic year of 1912: Was it exceptional?, *Weather*, *69*(4), 100–104, doi:10.1002/wea.2238.
- Bigg, G. R., M. R. Wadley, D. P. Stevens, and J. A. Johnson (1997), Modelling the dynamics and thermodynamics of icebergs, *Cold Reg. Sci. Technol.*, *26*(2), 113–135, doi:10.1016/S0165-232X(97)00012-8.
- Broström, G., A. Melsom, M. Sayed, and I. Kubat (2009), Iceberg modeling at met.no: Validation of iceberg model, *met.no Rep.* 17, Norw. Meteorol. Inst., Oslo, Norway.
- Crépon, M., M. N. Houssais, and B. S. Guily (1988), The drift of icebergs under wind action, *J. Geophys. Res.*, *93*(C4), 3608–3612, doi:10.1029/JC093iC04p03608.
- Depoorter, M. A., J. L. Bamber, J. A. Griggs, J. T. M. Lenaerts, S. R. M. Ligtenberg, M. R. van den Broeke, and G. Moholdt (2013), Calving fluxes and basal melt rates of Antarctic ice shelves, *Nature*, *502*, 89–92, doi:10.1038/nature12567.
- Duprat, L. P. A. M., G. R. Bigg, and D. J. Wilton (2016), Enhanced Southern Ocean marine productivity due to fertilization by giant icebergs, *Nat. Geosci.*, *9*, 219–221, doi:10.1038/ngeo2633.
- Gladstone, R. M., G. R. Bigg, and K. W. Nicholls (2001), Iceberg trajectory modeling and meltwater injection in the Southern Ocean, *J. Geophys. Res.*, *106*(C9), 19,903–19,915, doi:10.1029/2000JC000347.
- Hellmer, H., and D. Olbers (1989), A two-dimensional model for the thermohaline circulation under an ice shelf, *Antarct. Sci.*, *1*, 325–336, doi:10.1017/S0954102089000490.
- Holland, D. M., and A. Jenkins (1999), Modeling thermodynamic ice–ocean interactions at the base of an ice shelf, *J. Phys. Oceanogr.*, *29*(8), 1787–1800, doi:10.1175/1520-0485(1999)029<1787:MTIOIA>2.0.CO;2.
- Hunke, E. C., and D. Comeau (2011), Sea ice and iceberg dynamic interaction, *J. Geophys. Res.*, *116*, C05008, doi:10.1029/2010JC006588.
- Jacobs, S. S., H. H. Hellmer, C. S. M. Doake, A. Jenkins, and R. M. Frolich (1992), Melting of ice shelves and the mass balance of Antarctica, *J. Glaciol.*, *38*, 375–387, doi:10.3198/1992JoG38-130-375-387.
- Jenkins, A. (1991), A one-dimensional model of ice shelf–ocean interaction, *J. Geophys. Res.*, *96*(C11), 20,671–20,677, doi:10.1029/91JC01842.
- Jenkins, A., and D. M. Holland (2007), Melting of floating ice and sea level rise, *Geophys. Res. Lett.*, *34*, 791–813, doi:10.1029/2007GL030784.
- Jongma, J. I., E. Driesschaert, T. Fichefet, H. Goosse, and H. Renssen (2009), The effect of dynamic–thermodynamic icebergs on the Southern Ocean climate in a three-dimensional model, *Ocean Modell.*, *26*, 104–113, doi:10.1016/j.ocemod.2008.09.007.
- Jung, T., et al. (2016), WWRP polar prediction project—Implementation plan for the year of polar prediction (YOPP) V2.0, *WWRP/PPP 4*, World Meteorol. Organ., Geneva, Switzerland.
- Keghouche, I., L. Bertino, and K. A. Lisæter (2009), Parameterization of an iceberg drift model in the Barents Sea, *J. Atmos. Oceanic Technol.*, *26*(10), 2216–2227, doi:10.1175/2009JTECHO678.1.
- Large, W. G., and S. G. Yeager (2009), The global climatology of an interannually varying air–sea flux data set, *Clim. Dyn.*, *33*(2), 341–364, doi:10.1007/s00382-008-0441-3.
- Lichey, C., and H. Hellmer (2001), Modeling giant iceberg drift under the influence of sea ice in the Weddell Sea, *J. Glaciol.*, *158*, 452–460, doi:10.3189/172756501781832133.
- Marsh, R., et al. (2015), NEMO–ICB (v1.0): Interactive icebergs in the NEMO ocean model globally configured at eddy-permitting resolution, *Geosci. Model Dev.*, *8*(5), 1547–1562, doi:10.5194/gmd-8-1547-2015.
- Martin, T., and A. Adcroft (2010), Parameterizing the fresh-water flux from land ice to ocean with interactive icebergs in a coupled climate model, *Ocean Modell.*, *34*, 111–124, doi:10.1016/j.ocemod.2010.05.001.

- Merino, N., J. L. Sommer, G. Durand, N. C. Jourdain, G. Madec, P. Mathiot, and J. Tournadre (2016), Antarctic icebergs melt over the Southern Ocean: Climatology and impact on sea ice, *Ocean Modell.*, *104*, 99–110, doi:10.1016/j.ocemod.2016.05.001.
- Neshyba, S., and E. G. Josberger (1980), On the estimation of Antarctic iceberg melt rate, *J. Phys. Oceanogr.*, *10*(10), 1681–1685, doi:10.1175/1520-0485(1980)010<1681:OTEAI>2.0.CO;2.
- Orsi, A. H., T. Whitworth, and W. D. Nowlin (1995), On the meridional extent and fronts of the Antarctic Circumpolar Current, *Deep Sea Res., Part I*, *42*, 641–673, doi:10.1016/0967-0637(95)00021-W.
- Rackow, T. (2011), Modellierung der Eisbergdrift als Erweiterung eines Finite-Elemente-Meeris-Ozean-Modells, diploma thesis, Univ. of Bremen, Alfred Wegener Inst., Helmholtz Cent. for Polar and Mar. Res., Bremerhaven, Germany, doi:10013/epic.39071.
- Rackow, T., H. F. Goessling, T. Jung, D. Sidorenko, T. Semmler, D. Barbi, and D. Handorf (2016a), Towards multi-resolution global climate modeling with ECHAM6-FESOM. Part II: Climate variability, *Clim. Dyn.*, 1–26, doi:10.1007/s00382-016-3192-6.
- Rackow, T., C. Wesche, R. Timmermann, H. H. Hellmer, S. Juricke, and T. Jung (2016b), Melt climatology estimates for small to giant Antarctic icebergs, links to NetCDF files, PANGAEA Data Center, Bremerhaven, Germany, doi:10.1594/PANGAEA.865335.
- Schodlok, M. P., H. H. Hellmer, G. Rohardt, and E. Fahrbach (2006), Weddell sea iceberg drift: Five years of observations, *J. Geophys. Res.*, *111*, C06018, doi:10.1029/2004JC002661.
- Schourup-Kristensen, V., D. Sidorenko, D. A. Wolf-Gladrow, and C. Völker (2014), A skill assessment of the biogeochemical model REcoM2 coupled to the finite element sea ice–ocean model (FESOM 1.3), *Geosci. Model Dev.*, *7*(6), 2769–2802, doi:10.5194/gmd-7-2769-2014.
- Sidorenko, D., et al. (2015), Towards multi-resolution global climate modeling with ECHAM6-FESOM. Part I: Model formulation and mean climate, *Clim. Dyn.*, *44*(3), 757–780, doi:10.1007/s00382-014-2290-6.
- Silva, T. A. M., G. R. Bigg, and K. W. Nicholls (2006), Contribution of giant icebergs to the Southern Ocean freshwater flux, *J. Geophys. Res.*, *111*, C03004, doi:10.1029/2004JC002843.
- Smith, S. D. (1993), Hindcasting iceberg drift using current profiles and winds, *Cold Reg. Sci. Technol.*, *22*(1), 33–45, doi:10.1016/0165-232X(93)90044-9.
- Smith, S. D., and E. G. Banke (1983), The influence of winds, currents and towing forces on the drift of icebergs, *Cold Reg. Sci. Technol.*, *6*(3), 241–255, doi:10.1016/0165-232X(83)90045-9.
- Stern, A., A. Adcroft, and O. Sergienko (2016), The effects of Antarctic iceberg calving-size distribution in a global climate model, *J. Geophys. Res. Oceans*, *121*, 5773–5788, doi:10.1002/2016JC011835.
- Stern, A. A., E. Johnson, D. M. Holland, T. J. Wagner, P. Wadhams, R. Bates, E. P. Abrahamson, K. W. Nicholls, A. Crawford, J. Gagnon, and J.-E. Tremblay (2015), Wind-driven upwelling around grounded tabular icebergs, *J. Geophys. Res. Oceans*, *120*(8), 5820–5835, doi:10.1002/2015JC010805.
- Stuart, K., and D. Long (2011), Tracking large tabular icebergs using the seawinds Ku-band microwave scatterometer, *Deep Sea Res., Part II*, *58*(11–12), 1285–1300, doi:10.1016/j.dsr.2010.11.004.
- Tamura, T., K. I. Ohshima, A. D. Fraser, and G. D. Williams (2016), Sea ice production variability in Antarctic coastal polynyas, *J. Geophys. Res. Oceans*, *121*, 2967–2979, doi:10.1002/2015JC011537.
- Timmermann, R., S. Danilov, J. Schröter, C. Böning, D. Sidorenko, and K. Rollenhagen (2009), Ocean circulation and sea ice distribution in a finite element global sea ice–ocean model, *Ocean Modell.*, *27*(3–4), 114–129, doi:10.1016/j.ocemod.2008.10.009.
- Timmermann, R., Q. Wang, and H. H. Hellmer (2012), Ice shelf basal melting in a global finite-element sea ice–ice shelf–ocean model, *Ann. Glaciol.*, *53*(60), 303–314, doi:10.3189/2012AoG60A156.
- Turnbull, I. D. (2010), Drift of large tabular icebergs in response to atmospheric surface pressure gradients, an observational study, *Antarct. Sci.*, *22*(2), 199–208, doi:10.1017/S0954102010000027.
- Wang, Q., S. Danilov, D. Sidorenko, R. Timmermann, C. Wekerle, X. Wang, T. Jung, and J. Schröter (2014), The finite element sea ice–ocean model (FESOM) v.1.4: Formulation of an ocean general circulation model, *Geosci. Model Dev.*, *7*(2), 663–693, doi:10.5194/gmd-7-663-2014.
- Weeks, W. F., and M. Mellor (1978), Some elements of iceberg technology, in *Proceedings of the First Conference on Iceberg Utilization for Freshwater Production*, edited by A. A. Husseiny, pp. 45–98, Iowa State Univ., Ames.
- Wesche, C., and W. Dierking (2015), Near-coastal circum-Antarctic iceberg size distributions determined from Synthetic Aperture Radar images, *Remote Sens. Environ.*, *156*, 561–569, doi:10.1016/j.rse.2014.10.025.
- Wesche, C., D. Jansen, and W. Dierking (2013), Calving fronts of Antarctica: Mapping and classification, *Remote Sens.*, *5*(12), 6305–6322, doi:10.3390/rs5126305.